

## Electromagnetic images of a volcanic zone

Alan G. Jones <sup>\*,a</sup>, Isabelle Dumas <sup>b</sup>

<sup>a</sup> Geological Survey of Canada, 1 Observatory Crescent, Ottawa, Ont., K1A 0Y3 Canada

<sup>b</sup> Génie Minéral, Ecole Polytechnique de Montréal, CP 6079 Suc. A, Montréal, Qué., H3C 3A7 Canada

(Received 8 November 1992; revision accepted 15 March 1993)

### ABSTRACT

Data from 20 magnetotelluric (MT) soundings in the Coast belt of southwestern British Columbia, Canada, in the vicinity of volcanic Mounts Meager and Cayley (approximately 150 km north of Vancouver), are analysed to determine both the internal electrical conductivity structure of the Garibaldi volcanic belt and the regional conductivity structure. Galvanic distortion effects on the data are removed using Groom–Bailey tensor decomposition, and the regional 2D responses are determined in a survey-consistent reference coordinate frame for 1D and 2D modelling and inversion. The remaining unknowns, the site gain at each location, are estimated by requiring the long-period asymptotes of the *E*-polarization  $\rho_a$  curves to be the same, and alternatively are derived as part of the 2D inversion procedure. Positive correlations are observed between an increased temperature gradient at a depth of about 200 m, a zone of enhanced electrical conductivity and drilling results. The zone of enhanced conductivity is interpreted to be due to montmorillonite-dominated clay alteration minerals which form the cap rock of the geothermal reservoir. Below this cap, the zone is electrically resistive owing to the chlorite and sericite which form the reservoir itself. The volcanic belt is underlain by highly resistive (more than 10 000  $\Omega$  m) crystalline rock, beneath which is a deep conductive region (less than 70  $\Omega$  m) beginning at a depth of 12 km. The cause of this crustal zone of enhanced conductivity is thought to be free saline water possibly released by metamorphic devolatilization from the downgoing Juan de Fuca slab. Within this conductive layer is a region of high conductivity directly beneath the volcanic belt, which we interpret as the magma source body for the belt. Sensitivity studies imply that the upper crustal resistive zone underlies the whole complex, although a weakly conductive, thin, vertical channel, representative of a magma conduit from the deep source body to the near surface, cannot be excluded.

### 1. Introduction

Magmatic activity associated with the downgoing Juan de Fuca plate beneath northwestern North America (Fig. 1) causes hot springs and high geothermal gradients in the Garibaldi volcanic belt of southwestern British Columbia (Fig. 2). More spectacularly, it can lead to volcanic eruptions, such as the 1980 Mount St. Helens event in the Cascadia volcanic front, which is the extension of the Garibaldi belt in the state of Washington. The Garibaldi belt has been studied geoscientifically since the early 1970s as part of a

national programme (Federal Geothermal Energy Program) to identify potential geothermal energy resources. In particular, studies have been undertaken in the vicinity of Mount Cayley and Mount Meager, 150 km north of Vancouver, to determine the structural geometry of the geothermal reservoirs (Lewis and Souther, 1978).

The basement rocks of the region are part of the Coast belt (Fig. 1), a plutonic complex of Tertiary and older granitic and associated metamorphic rocks. In the Mount Meager area (Fig. 2), the complex is comprised of fractured granodiorite and associated gneiss, and is crossed by a NNW-trending belt of late Tertiary and Quaternary plutons, and a north–south belt (Garibaldi)

\* Corresponding author.

of Quaternary volcanoes of andesite–dacite composition. The most recent eruption of Mount Meager occurred approximately 2350 years B.P.

(Read, 1990), and is thought to have been as large as the 1980 Mount St. Helens event (Hickson, 1993).

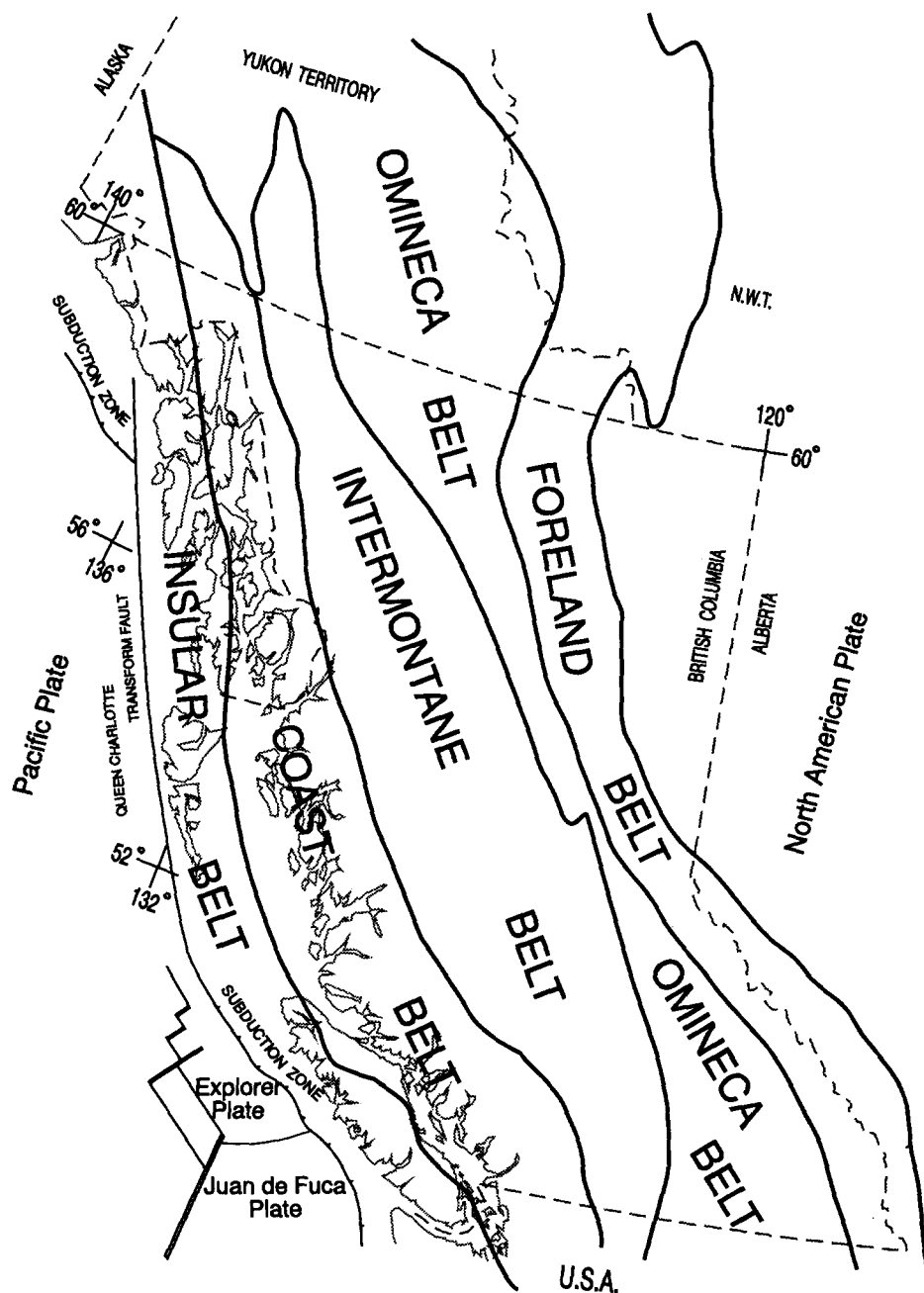


Fig. 1. Map of the Canadian Cordillera showing the five morphogeological belts and the plate boundaries off British Columbia's west coast.

Magnetotelluric (MT) data acquired in the early 1980s close to Mounts Meager and Cayley, combined with data acquired under the auspices of LITHOPROBE in 1989, provide a set of 20 sites (Fig. 3) which can be interpreted for both regional conductivity structure and the internal

conductivity structure of the geothermal and volcanic environments. In this paper, we analyse, model, and interpret these data using the most current MT processing and inversion techniques. The effects of galvanic distortions caused by local, near-surface inhomogeneities are removed by

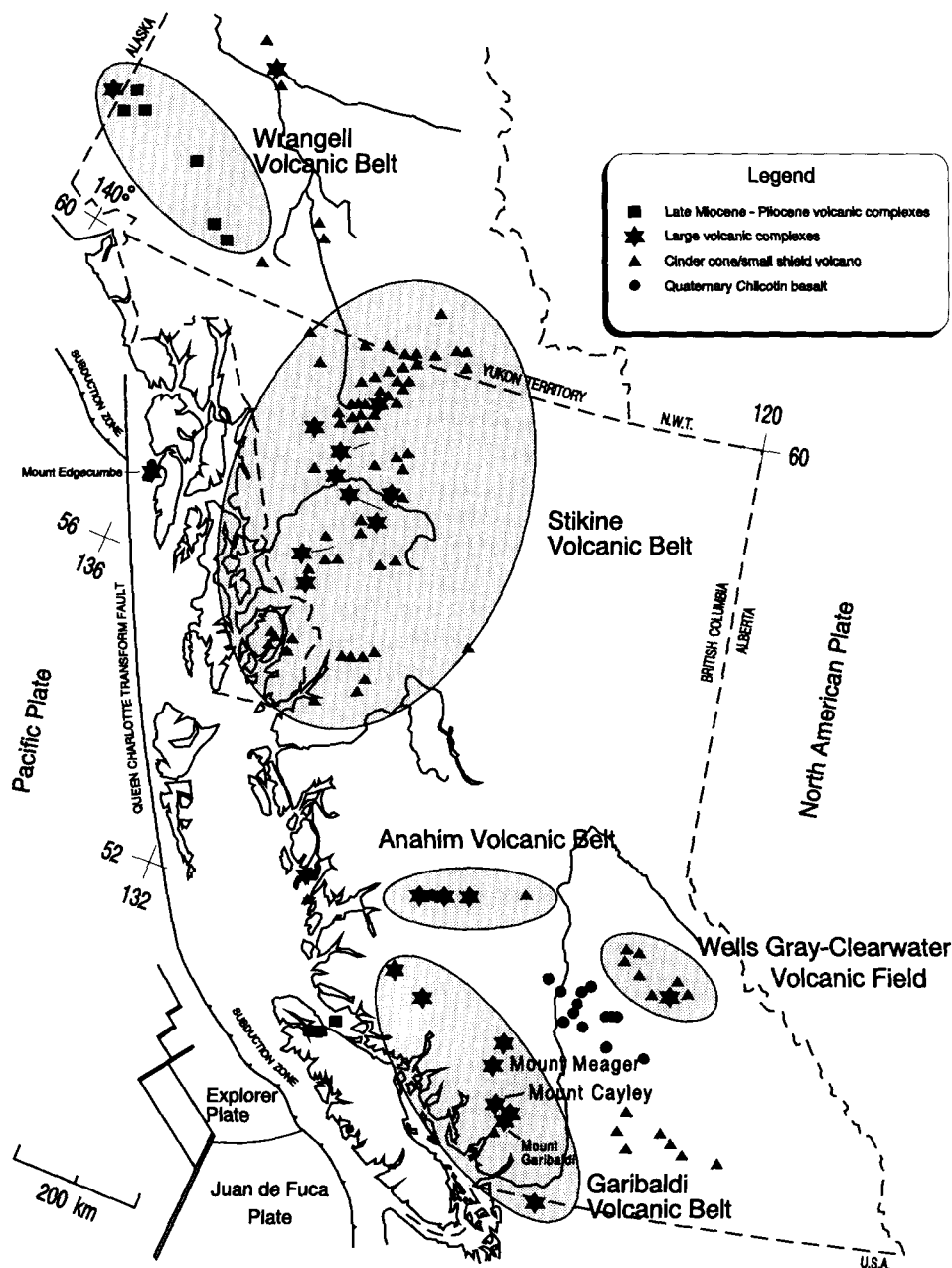


Fig. 2. Volcanic zones in the Canadian Cordillera.

undertaking tensor decomposition. The corrected data are inverted for 1D models, and are both forward modelled and inverted using 2D codes. From the resulting models we draw conclusions regarding the physical characteristics of the geothermal field, the dimensions of the volcanic belt, and the possible location of the magma source body.

## 2. Geological setting

### 2.1. Regional setting

The Canadian Cordillera extends north from the US border to the Beaufort Sea, and east from

the Pacific Ocean and Alaska to the Interior Plains (Fig. 1). The region comprises five major NW-trending morphogeological belts, each with its own distinctive stratigraphy, metamorphism, plutonism, volcanism, and structure: the Foreland belt, the Omineca belt, the Intermontane belt, the Coast belt, and the Insular belt (Fig. 1). The tectonic evolution of the Canadian Cordillera encompassed a wide variety of processes, including the following: (1) development of a miogeoclinal succession along the rifted passive margin of western ancestral North America beginning in Middle Proterozoic time; (2) an orogenic event which resulted in rifting, volcanism and plutonism in the outer part of the miogeocline in Late Devonian time; (3) the amalgamation and accre-

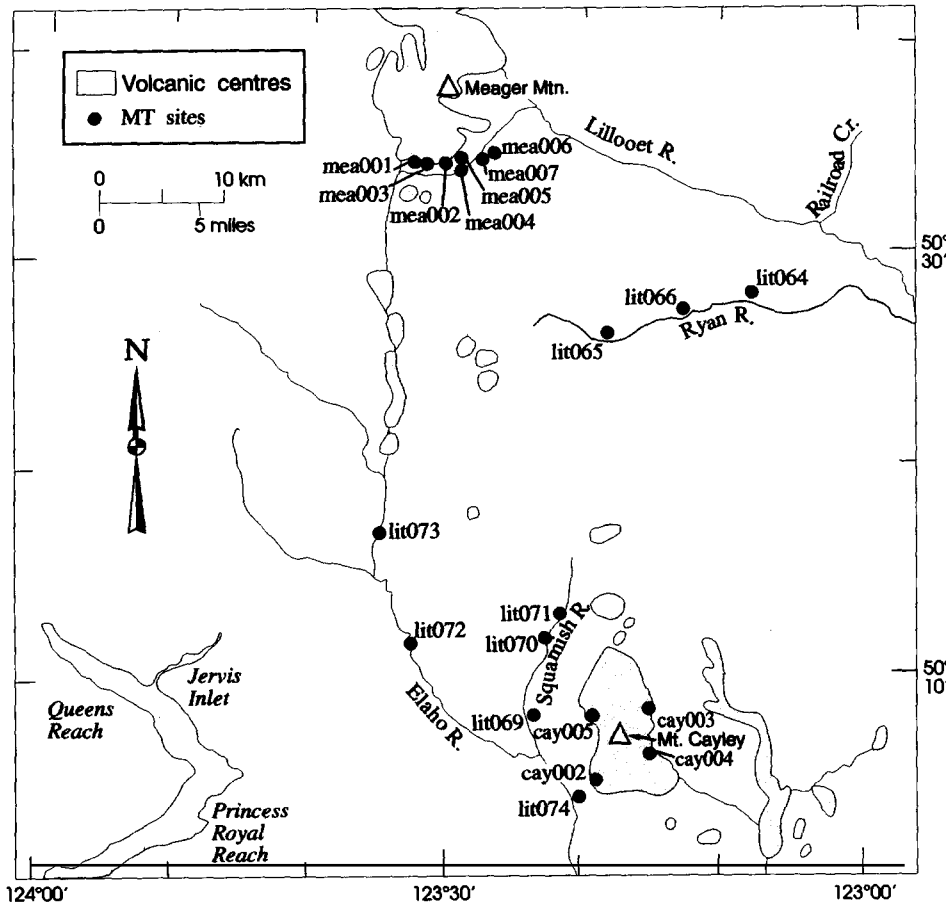


Fig. 3. MT site locations and the Mount Meager and Mount Cayley volcanic fields.

tion of volcanic, island arc and oceanic terranes with deformation, metamorphism, volcanism and plutonism during Mesozoic and Cenozoic time; (4) major displacements along dextral transcurrent faults during Cretaceous and Cenozoic time (Gabrielse and Yorath, 1989).

The distribution of earthquakes, active and recently active faults, and young volcanoes in the Canadian Cordillera is controlled by the motions of the Pacific, North American, Juan de Fuca, and Explorer plates (Fig. 1), which are in contact in the NE Pacific Ocean west of British Columbia. The current rate of convergence of the Juan de Fuca (JdF) and North American plates is estimated at 5–6 cm year<sup>-1</sup> (Riddihough, 1978), and seismic and gravity studies suggested that the JdF plate has a shallow dip of 8–16° under Vancouver Island (Spence et al., 1985). This has been confirmed by more recent seismicity (Hyndman, 1988; Hyndman et al., 1990), seismic reflection (Clowes et al., 1987), and shear wave (Cassidy and Ellis, 1991, 1993) studies which trace the top of the downgoing oceanic plate to depths of more than 60 km beneath Georgia Strait on British Columbia's west coast between the mainland and Vancouver Island.

Within the Canadian Cordillera several hundred volcanoes have been active during the last 2 m.y. Tectonically, the volcanoes of the Canadian Cordillera can be divided into volcanic belts (Fig. 2) which have had volcanic eruptions and other tectonically less well-defined cones and cone fields (Hickson, 1993). These are, from north to south:

(1) the Wrangell volcanic belt in the western Yukon and Alaska, which are related to subduction (Richter et al., 1990).

(2) The Stikine belt of northwestern British Columbia and southeastern Yukon, which contains more than 50 Quaternary eruptive centres, at least one of which is younger than 150 years old. This belt appears to be the result of continental rifting (Souther, 1992).

(3) The Anahim belt, which extends in an east–west direction across western British Columbia at about 52°N, includes about 30 Quaternary volcanoes of mainly basaltic composition. This belt may be the product of progressive

movement of the North American plate over one or more hotspots in the mantle (Souther, 1986).

(4) The Garibaldi volcanic belt, which is the southernmost, is the northern extension of a well-defined chain of late Cenozoic volcanoes in northern California, Oregon, and Washington (Cascade belt). It contains more than 30 Quaternary cones and domes of andesite and minor basalt, which probably formed in response to subduction of the Juan de Fuca and Explorer plates off the coast of Vancouver Island (Green et al., 1988).

In this paper, we will study the Garibaldi volcanic belt in more detail using surface electromagnetic (EM) measurements.

## 2.2. Local setting

The region of interest in this study, the volcanic Garibaldi belt, is located within British Columbia's Coast belt. According to Roddick (1983), the Coast belt is one of the largest Phanerozoic granitic complexes in the world. It consists of Jurassic to Tertiary granitic rocks and variably metamorphosed sedimentary and volcanic strata ranging in age from Palaeozoic to early Tertiary. The plutonic rocks are relatively mafic, with quartz diorite forming about 40% of the total plutonic rock and tonalite and diorite together another 30% (Monger, 1989).

The Coast belt formed mainly during the Cretaceous and early Tertiary, probably as a result of the collision of amalgamated terranes of the Intermontane belt with a large composite terrane to the west (the Insular belt). Compressional thickening and tectonic overlap resulting from this collision have been invoked to explain 5–25 km of uplift and erosion that occurred along the axis of the belt in Cenozoic time (Clague, 1989).

In the area of acquisition on Mount Meager, the complex consists of fractured granodiorite and associated gneiss. It is crossed by a NNW-trending belt of late Tertiary and Quaternary plutons and a north–south belt of Quaternary volcanoes of andesite–dacite composition (Read, 1978, 1990). The most recent eruption of Mount Meager was approximately 2350 years ago, and Pleistocene alluvium of volcanic origin overlay

both basement and volcanic material. Read (1977) described the nine volcanic assemblages composing the complex of Meager Creek.

### 3. MT data and analyses

#### 3.1. Data

The MT data for this study are concentrated in the region of Mount Meager (50°34'N, 123°23'W) and Mount Cayley (50°7'N, 123°17'W) (Fig. 3). Acquisition of these data was undertaken both in-house (Mount Meager sites), and by commercial contract, and was funded as part of two programmes: the Federal Geothermal Energy Program of the early 1980s and the GSC/NSERC LITHOPROBE program of the late 1980s. Around Mount Meager (Fig. 3) seven MT sounding (mea001–mea007) were measured in 1983–1984 along an east–west traverse crossing the South Thermal Reservoir geothermal anomaly near Meager Creek 150 km north of Vancouver, and in 1983 four MT soundings (cay002–cay005) were measured near Mount Cayley (Site cay001 produced no useful data). In addition, MT data from nine sites (lit064–lit066 and lit069–lit074), acquired as part of LITHOPROBE's Southern Cordilleran transect investigations (Jones et al., 1992a), were included to determine the regional electrical conductivity structure.

#### 3.2. Previous electrical and EM results

The Mount Meager and Mount Cayley areas have been studied extensively since the mid-1970s using a variety of electrical and EM methods (see Flores et al., 1985; Flores-Luna, 1986). In the mid-1970s, scalar MT data from sites around both volcanoes were interpreted, using 1D layered-Earth models, by Pham Van Ngoc (1977, 1978, 1980), who concluded that the data showed the existence of conductive zones at shallow levels (2 km for Mount Meager and 6 km for Mount Cayley) beneath the two volcanic zones. These zones were interpreted as magma chambers by Pham van Ngoc (1980). Although the data, analyses, and interpretation were, by modern stan-

dards, crude, the significant information that conductive zones lie beneath each volcanic zone was obtained.

The MT data from the seven sites across the South Thermal Reservoir on Mount Meager (mea001–mea007) have previously been interpreted by Flores et al. (1985), who undertook 1D layered-Earth inversions of the 'E-polarization' data rotated into a coordinate system with the telluric component in a NW–SE direction. Flores et al. (1985) concluded that, with the exception of the data from Site mea-001 (for which the 'B-polarization' data were inverted), all other Mount Meager MT data indicated the existence of a conducting zone beneath the South Thermal Reservoir at depths of around 200 m.

DeLaurier (1986) undertook 1D and 2D modelling of the Mount Cayley data, and concluded that a conductive block of width 6–7 km, thickness 2–6 km, and resistivity 1  $\Omega$ m underlies the mountain at a depth of 1 km. DeLaurier (1986) attempted to interpret this anomaly in terms of a 1% saline-fluid saturated granite. Long-period MT data from three sites close to Mount Meager were interpreted one-dimensionally by Dragert et al. (1980), who concluded that a good conducting zone (less than 100  $\Omega$  m) underlies the highly resistive (greater than 10 000  $\Omega$  m) crystalline complex at a depth of 20 km.

#### 3.3. Transfer functions and induction arrows

Geomagnetic depth sounding (GDS) transfer functions relate the vertical magnetic field component to the horizontal magnetic components. The transfer functions are computed at each frequency, and are separated into in-phase (real) and quadrature (imaginary) components. Transfer functions are relatively unaffected by small-scale anomalies that distort electric field amplitudes, and therefore are robust indicators of regional conductivity structure. One representation of these transfer functions is as real and imaginary induction arrows, or Parkinson arrows (Parkinson, 1962). The real arrows, when reversed, generally point towards zones of enhanced conductivity (Jones, 1986) and can be used to locate lateral changes in resistivity.

Transfer functions were computed for a wide range of frequencies at each site to locate spatially the conductive zone. The resulting in-phase induction arrows at the period of greatest response (frequency 3 Hz) are shown in Fig. 4. The induction arrows clearly point towards the Garibaldi volcanic belt, which has a strike of N10–15°W. The arrows also indicate that the regional response can be characterized by a 2D resistivity model.

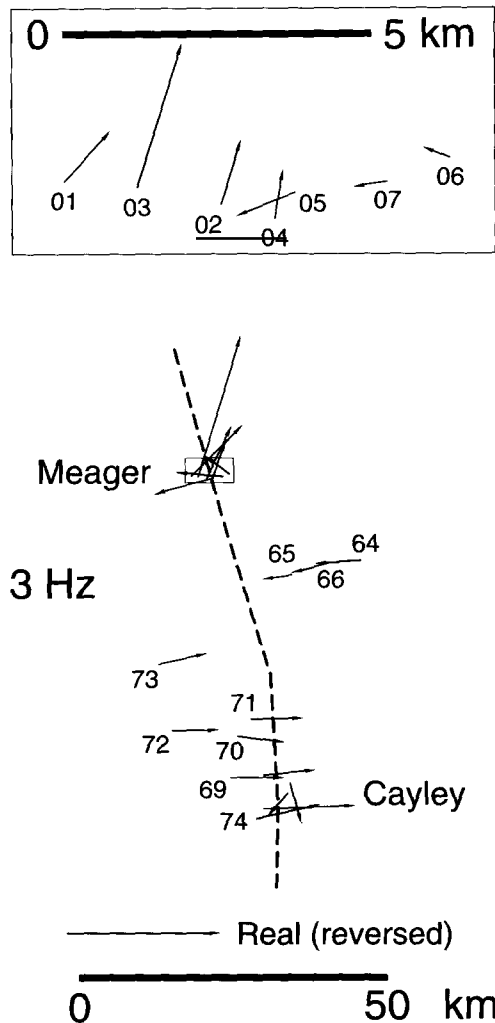


Fig. 4. Real induction arrows at 0.33 s period (frequency of 3 Hz). The dashed line shows the trace of the Garibaldi volcanic front. The inset shows the arrows from Mount Meager sites on an expanded scale.

### 3.4. Tensor decomposition

Local distortions of the electric field by near-surface inhomogeneities can have significant effects on the MT impedance tensors and must therefore be recognized and corrected (see, e.g. Groom and Bahr, 1992). A number of techniques have been proposed to deal with this problem using various mathematical and physical tensor decomposition approaches (Eggers, 1982; LaToraca et al., 1986; Zhang et al., 1986; Yee and Paulson, 1987; Bahr, 1988, 1991; Groom and Bailey, 1989a, 1991; Chakridi et al., 1992). Given its physically based decomposition, and that one can test statistically if the assumed distortion model is appropriate, we chose the Groom–Bailey (GB) decomposition method and applied it to the data.

The GB method tests quantitatively the hypothesis that the regional geoelectric structure can be characterized by a 2D model, with conductive or resistive near-surface 3D anomalies causing galvanic distortion of the Earth's electric fields. The goal is to determine the inherent dimensionality of the data, and, if 2D, to obtain a regional strike direction. The method fits the data, in a least-squares sense, to a model of telluric distortion, described by two frequency-independent real parameters (termed by GB twist and shear), of a regional 2D MT impedance tensor rotated into the observational frame of reference. Following Groom and Bailey (1989a, 1991), the MT impedance tensors at each frequency and at each station were analysed. Our method followed closely that described by Groom et al. (1993) and we illustrate with the data from Site mea007.

Figure 5(A) shows the fit of a 2D (Swift, 1967) parametrization of the data. The error statistic tests the model hypothesis, and is a  $\chi^2$ -like measure of misfit normalized by the data variance of each element of the impedance tensor such that a value in the range 0–4 indicates that the model fits to within two standard errors (on average) of each of the eight data (real and imaginary parts of each of the four elements in the MT impedance tensor). The error of misfit, for this 2D parametrization, lies above the acceptable level (four, shown by the solid line in the error plots)

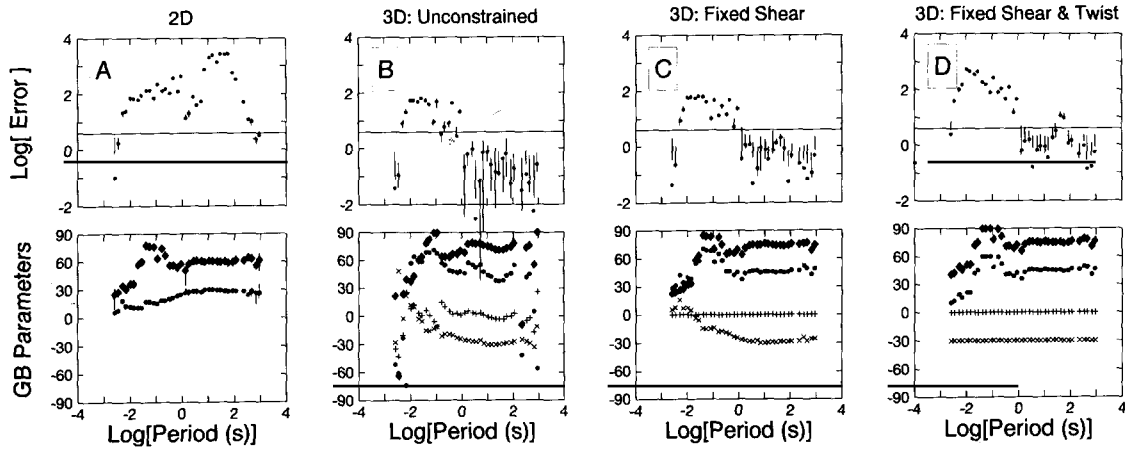


Fig. 5. Steps in the GB decomposition of MT data from Site mea007. The upper row illustrates the misfit error, and the lower row shows the distortion parameters determined. ♦ Regional strike; +, shear; ×, twist; ●, current channelling azimuth. (A) 2D (Swift) parametrization. (B) GB parametrization with all parameters permitted to vary with frequency. (C) GB parametrization with shear held constant at  $0^\circ$ . (D) GB parametrization with both shear and twist held constant, at  $0^\circ$  and  $-30^\circ$ , respectively.

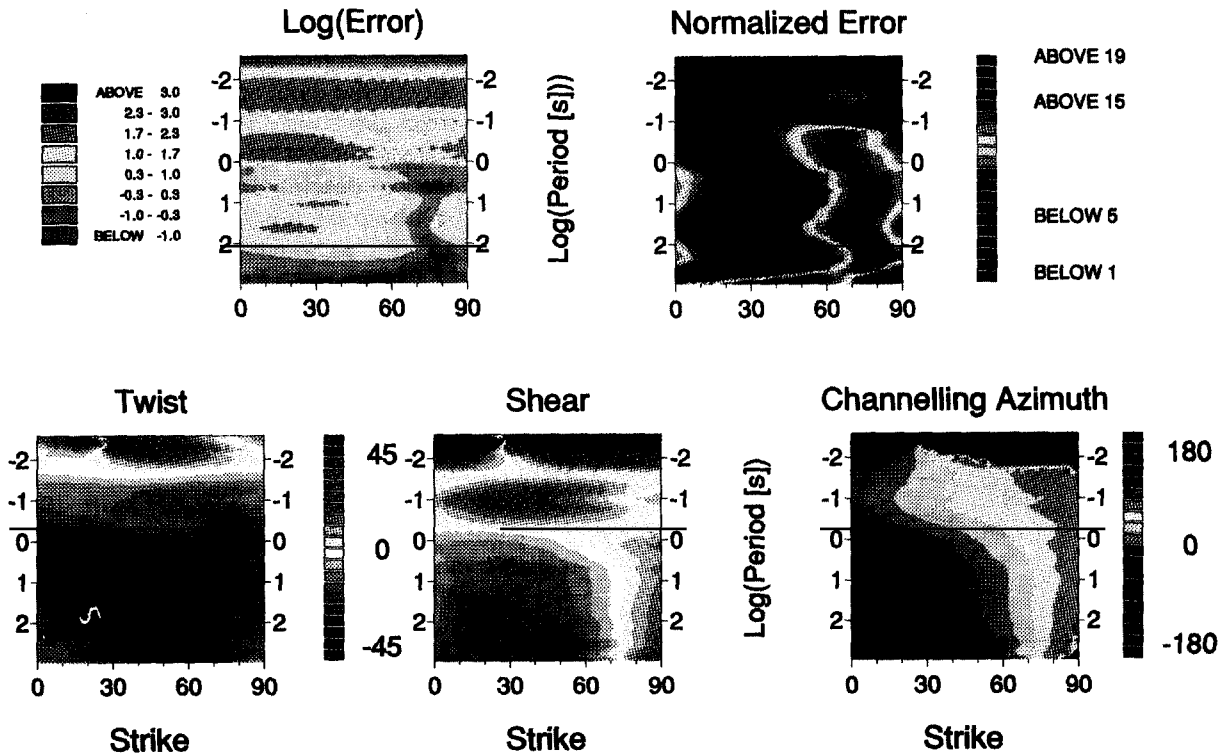


Fig. 6. Variation of the GB parameters with period and with rotation through  $0-90^\circ$ . Top left: log(misfit error). Values below 0.6 (blues and greens) fit the model well. Top right: normalized error. Values above 15 (reds) indicate best model fits. Bottom left: twist. Bottom centre: shear. Bottom right: channelling azimuth.



for virtually the whole period range. The 2D Swift strike direction is stable at periods longer than about 1 s and is  $+60^\circ$  (or  $-30^\circ$ , given the  $\pi/2$  ambiguity).

Figure 5(B) shows a GB parametrization permitting both the 3D telluric distortion parameters and the 2D regional strike to vary with period. Even in this parametrization, it is not possible to fit the model of 3D distortion acting on a 2D regional response at periods shorter than 0.1 s. This is due to the high-frequency 3D induction effects of the distorting body, which are also evident in the induction arrows (Fig. 4). At longer periods, however, the model fits to within the data errors. The next task is to constrain the strike and telluric distortion parameters so that they are frequency independent.

Inspection of the variation of the twist, shear and regional strike as the rotation angle is varied through  $0-90^\circ$  (Fig. 6) indicates that the most stable of the three is, for these data, the shear angle. As noted by Jones and Groom (1993) and Groom et al. (1993), it is usually the case that one

of the telluric distortion parameters is the most stable, and rare that the strike direction is sufficiently stable to warrant constraining it first in the decomposition procedure. The variation of the error of misfit with rotation (Fig. 6, top left) indicates that the lowest misfit is obtained when the regional strike angle is constrained in the range  $70-78^\circ$ . From the error we determine a normalized error given by a non-linear inverse mapping of the error which highlights regions close to the lowest (15–20) and highest (1–5) error, with best fit indicated by red, and worst fit by blue. This normalised error (Fig. 6, top right) illustrates that the most consistent best strike direction is  $70-78^\circ$ , whereas the worst strike direction is around  $30^\circ$ , the local current channelling azimuth (see Fig. 5(B)).

Figures 5(B) and 6 indicate that, for these data, the shear angle is the most robustly determined parameter at a value of around zero. Figure 5(C) shows the variation in the other model parameters when the shear angle is held constant at  $0^\circ$ ; clearly, holding the shear constant stabilizes

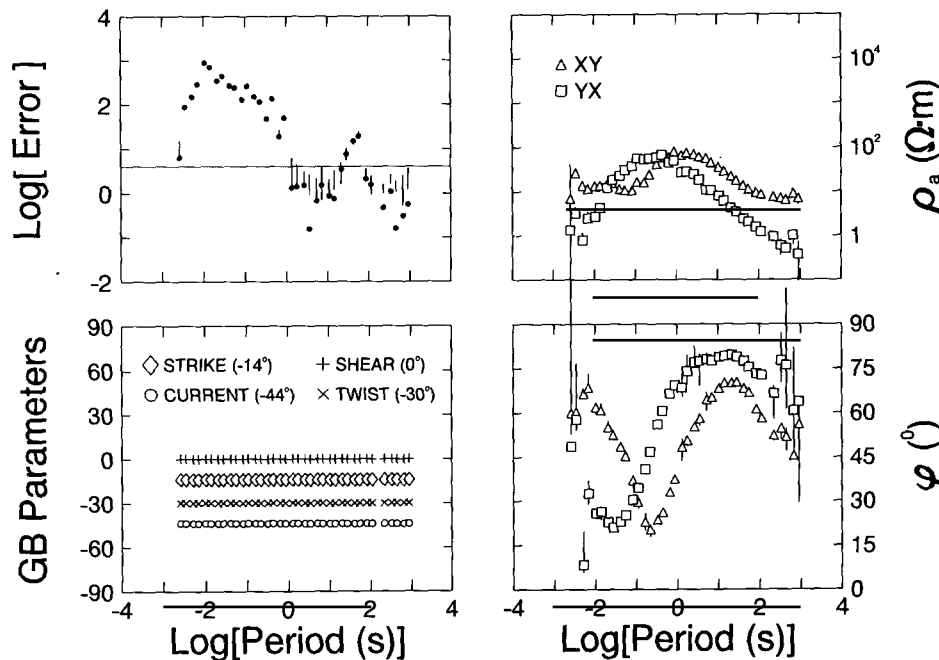


Fig. 7. Complete GB decomposition of mea007 with shear, twist and regional strike held constant (at  $0^\circ$ ,  $-30^\circ$  and  $-14^\circ$ , respectively) with period.

the other two parameters without increasing the misfit significantly. From Figure 5(C), one can estimate a value for twist, which exhibits less scatter than does regional strike, of  $-30^\circ$ . Figure 5(D) shows the misfit and 2D regional strike for both telluric parameters being held constant, with shear at  $0^\circ$  and twist at  $-30^\circ$ . At periods longer than 0.3 s the strike direction shows a preference for approximately  $75^\circ$ . Figure 7 displays the complete decomposition with the strike now held constant at  $-14^\circ$ ; there is a  $\pi/2$  ambiguity in the strike direction, and consideration of the  $\rho_a$  (apparent resistivity) curves and the induction arrows led us to define  $-14^\circ$  as the strike direction

rather than  $+76^\circ$ . This strike is consistent with the direction of the Garibaldi volcanic belt. It should be noted that the error is still acceptable at periods in excess of 1 s.

This analysis was applied to each site in turn; however, one must be careful when constraining either twist or shear before strike, as this leads to a coordinate system being imposed on the data (Groom et al., 1993). It is necessary to ensure that the strike direction derived is supported by the data, and is not one obtained by an inappropriate choice of twist and/or shear. Figure 8 displays the unconstrained GB strike directions determined from all frequencies at all 20 sites

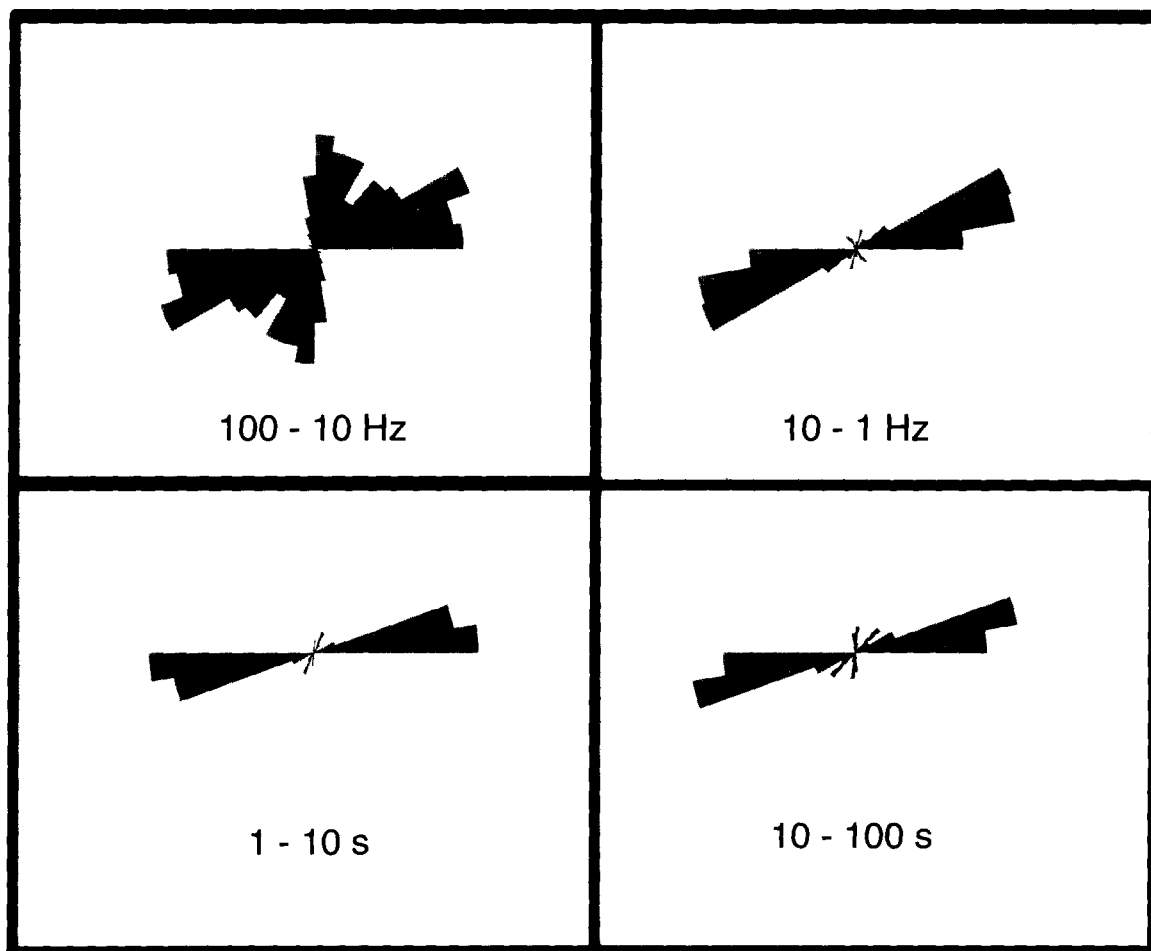


Fig. 8. GB strike for unconstrained fits from all 20 sites for all frequencies in the four period bands shown.

grouped into four period bands: 10–100 Hz, 1–10 Hz, 1–10 s, and 10–100 s. Clearly, all sites have a consistent strike direction of 75–85° at periods in excess of 10 Hz. The error contour plots from each site were averaged together, and a normalized average error contour plot was constructed (Fig. 9). Figure 9 concurs with Fig. 8 in showing that there is a survey-consistent strike direction of 75–85° (equivalent to  $-15^\circ$  to  $-5^\circ$ ) over much of the period range. In addition, the survey-consistent worst direction is 35–40°, which was the 2D parametrization strike direction at most sites. Accordingly, all data were decomposed with a fixed strike direction of  $-14^\circ$  and frequency-independent twists and shears (different for each site). In this coordinate frame, the *E*-polarization data are those for the electric currents flowing parallel to strike in a direction N14°W, whereas the *B*-polarization data are those for the currents

flowing perpendicular to strike in a direction N76°E.

It should be noted that the worst strike direction, given by the local current channelling azimuth of 35–40°, is close to that of N45°W adopted by Flores et al. (1985) in their interpretation of the Mount Meager data.

### 3.5. Site gain correction

After GB decomposition, there are two unresolved ‘static shift’ factors, which can be parametrized as an anisotropy tensor, with anisotropy coefficient  $s$ , multiplied by a site gain  $g$  (Groom and Bailey, 1989a). We correct for anisotropy by shifting the two  $\rho_a$  curves at each site, one for each mode, so that their high-frequency asymptotes match at a level given by their geometric means. The decomposed and

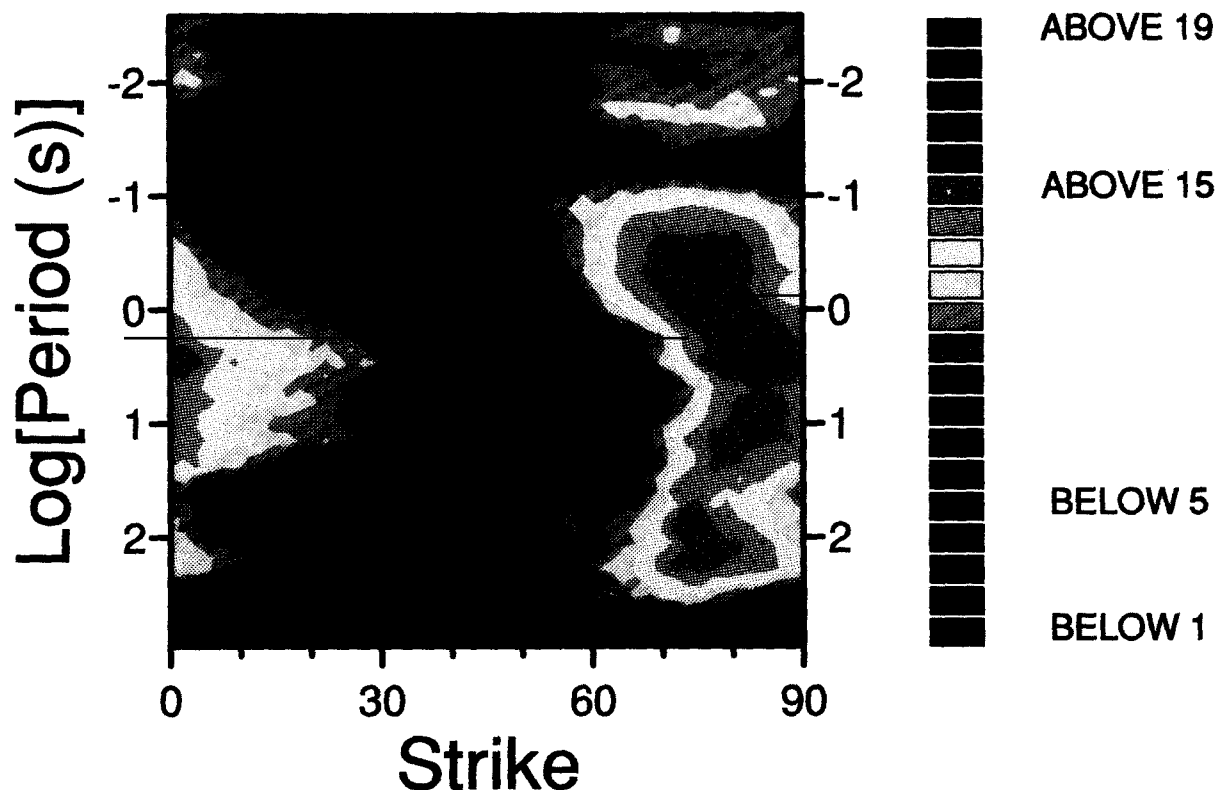


Fig. 9. Averaged normalized error plot derived from averaging the error plots from each of the 20 sites and normalizing.

anisotropy corrected MT data from all sites, classified into three groups (Mount Meager, Mount Cayley and Regional sites), are shown in Fig. 10. Although the  $\rho_a$  curves of these data require site gain corrections, the very high phases at high frequencies are evident for all Mount Meager

sites and for some of the Mount Cayley sites; these high phases are indicative of a shallow zone of enhanced conductivity.

Although, from theoretical studies, the site gain should be minor compared with the anisotropy (R. Groom, personal communication,

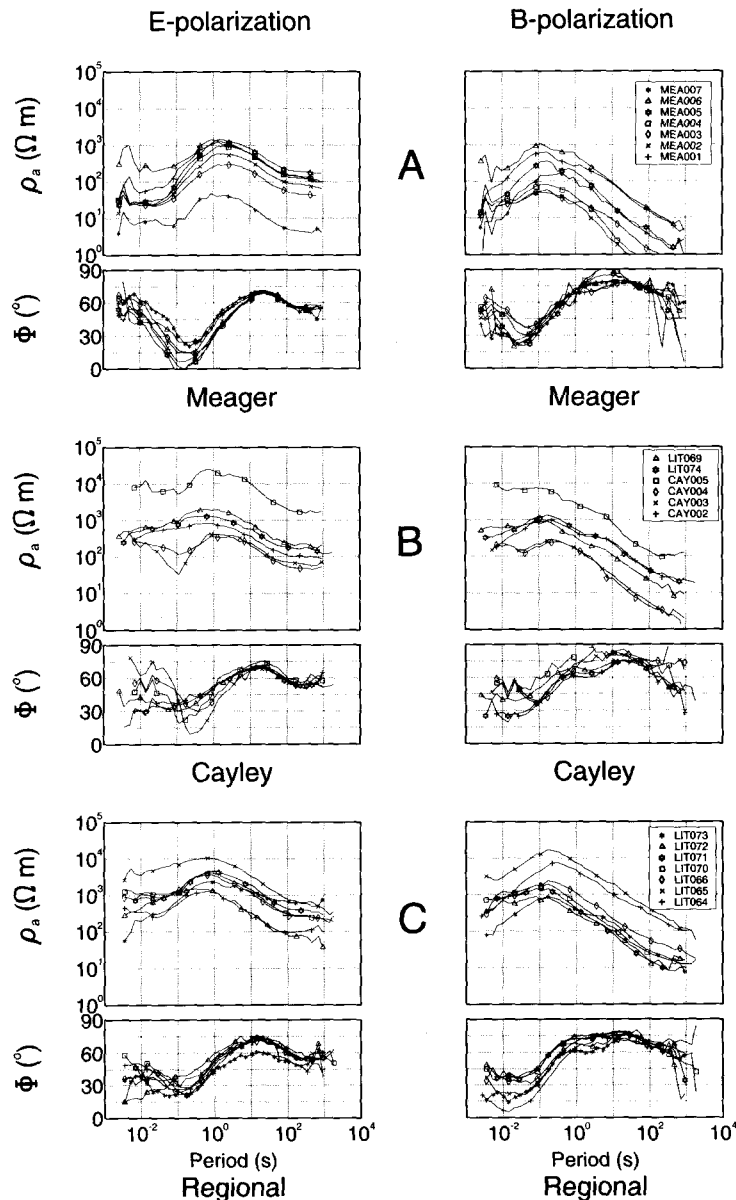


Fig. 10. MT data after GB decomposition and anisotropy correction. The *E*-polarization mode is for an electric field flowing 14° west of geographic north. (A) Sites on Mount Meager; (B) Sites on Mount Cayley; (C) Regional sites.

1991), it can still occasionally be of an order of magnitude, and hence must be corrected in some manner. In this paper, we apply two methods to try to correct for this site gain. One of these methods is performed as an integral part of the 2D inversion procedure, whereas the other is performed on the MT data themselves before 1D inversion and 2D forward modelling.

To correct the data for site gains before inversion, we considered the regional levels of the  $E$ -polarization  $\rho_a$  curves at periods which sample deeper than our region of interest; the top 10–20 km for this study. For periods in excess of 1 s, the skin depth of the EM fields from most sites is greater than 10 km. Thus, we conservatively chose 10 s as the period for deriving a regional level. Figure 11 shows the lateral variability of the  $\log(\rho_a)$  data for the  $E$ -polarization mode at 10 s from all 20 sites. The mean value of these data is about 600  $\Omega$  m, with a standard error of 260–1300  $\Omega$  m. It should be noted that there is virtually no regional trend evident (correlation coefficient for a linear regression of 0.15), and that of the 20

sites the majority fall within one-third of a decade of the mean value. A standard deviation of one-third of a decade for static shift was also evident in the data of Vanyan et al. (1989) from 2500 MT sites on the Siberian platform, and in the data of Sternberg et al. (1988) from MT sites in Oregon.

We then shifted both curves for each site simultaneously so that the  $E$ -polarization  $\rho_a$  datum had a value of 600  $\Omega$  m at 10 s. Such an approach, of deriving a regional or global resistivity curve from the profile and shifting the data to match this curve, has been used by others (e.g. Gordienko et al., 1981; Krasnobayeva et al., 1981; Warner et al., 1983; Vanyan et al., 1983; Berdichevsky et al., 1989).

Thus, the three steps to obtain our final data are as shown in Fig. 12 for Site mea007. Figure 12(A) shows the MT data in the local measurement axes. First, we remove the local telluric distortions and determine the data in the 2D regional strike direction (Fig. 12(B)). Then the anisotropy is corrected for by requiring the high-frequency part of the  $\rho_a$  curves to coalesce (Fig.

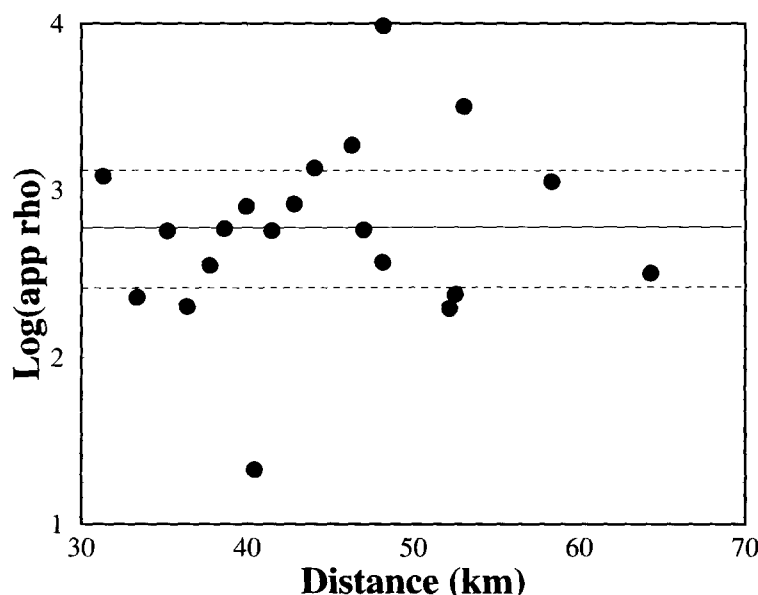


Fig. 11.  $E$ -Polarization  $\log(\rho_a)$  data at 10 s plotted against lateral distance from all 20 sites. The solid line represents the mean value of 600  $\Omega$  m, whereas the two dashed lines show  $\pm 1$  SD.

12(C)), and finally the local site gain is removed by shifting both curves simultaneously so that the *E*-polarization data are at a level of 600  $\Omega$  m at 10 s (Fig. 12(D)).

### 3.6. Contoured pseudosections

The corrected data are displayed in pseudo-section form in Fig. 13. The apparent resistivity pseudosections (Fig. 13, top two plots) show the reduced resistivities for sites on the volcanic front compared with the regional responses. The phase plots (Fig. 13, bottom two plots) show that there is little sensitivity in the *E*-polarization mode data (Fig. 13, bottom left plot) to lateral variation at periods in excess of 0.1 s. In contrast, the *B*-polarization phases (Fig. 13, bottom right plot)

exhibit a high of more than 80° at around 10 s period beneath the volcanic front sites. These high phases, and their associated low apparent resistivities, we found difficult to model.

## 4. Modelling and inversion

### 4.1. 1D inversion

As a preliminary step to 2D modelling and inversion, the shifted, decomposed *E*-polarization mode data were inverted for minimum 1D Earth structure using the Occam code of Constable et al. (1987). Figures 14(A)–14(C) show inversions for three sites, one off the flank of the volcanic front (lit072; Fig. 14(A)), one on Mount

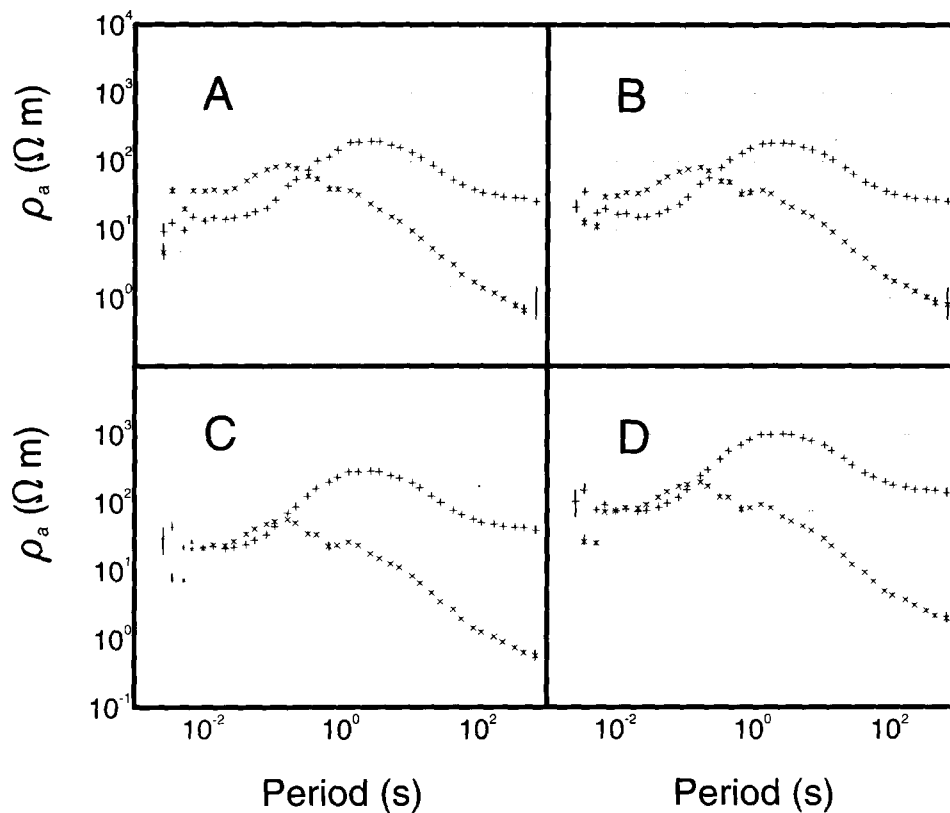


Fig. 12. Processing steps for the MT data illustrated for Site mea007. (A) Original data in measurement axes. (B) Data after removal of telluric distortions and rotated to a strike direction of  $-14^\circ$ . (C) Data corrected for anisotropy by requiring the high-frequency components to have the same level. (D) Correction for site gain by shifting both curves simultaneously such that the *E*-polarization data are at a level of 600  $\Omega$  m at 10 s.

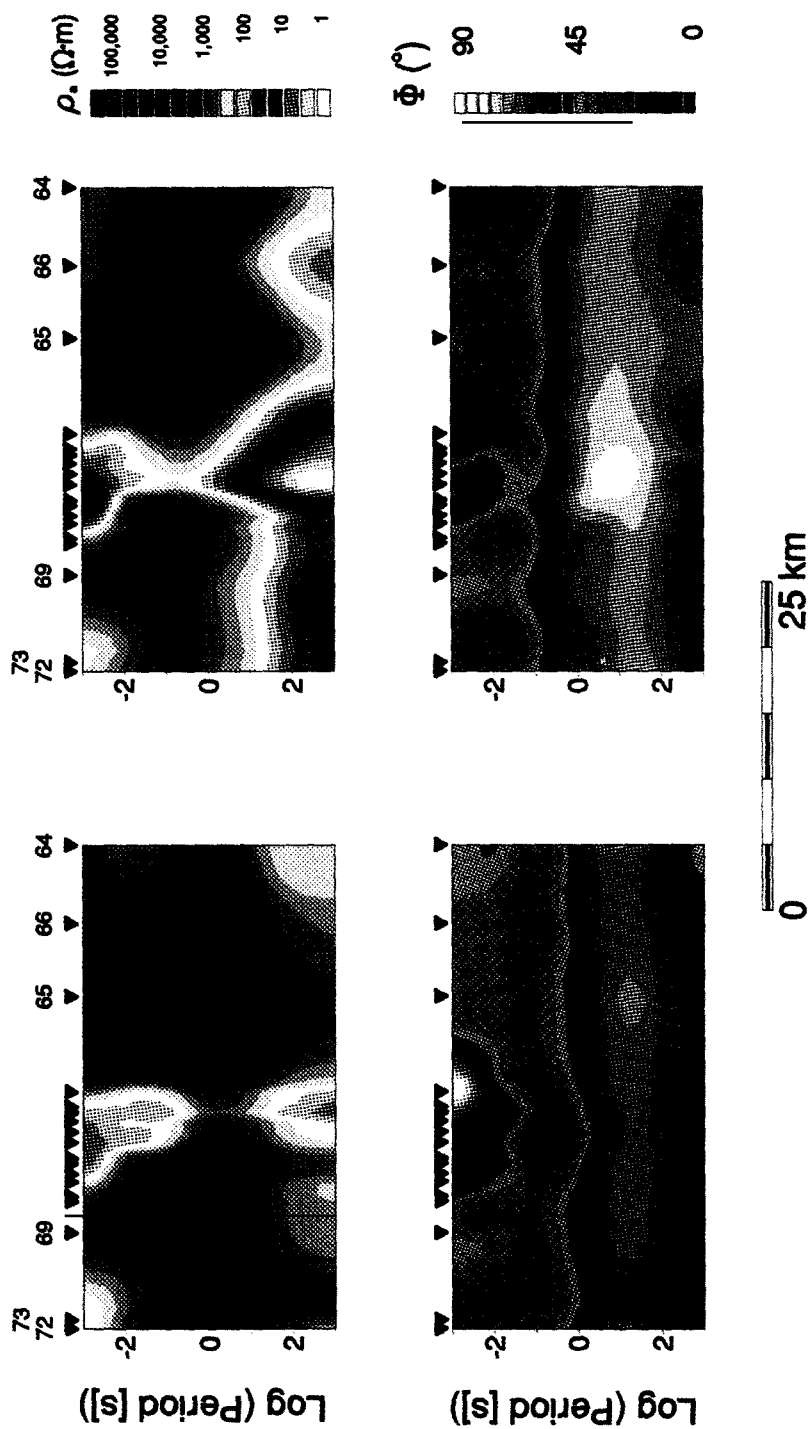


Fig. 13. Pseudosections of the MT data after decomposition and gain correction processing. Top row: apparent resistivity pseudosections; bottom row: phase pseudosections; left column:  $E$ -polarization mode data; right column:  $B$ -polarization mode data.

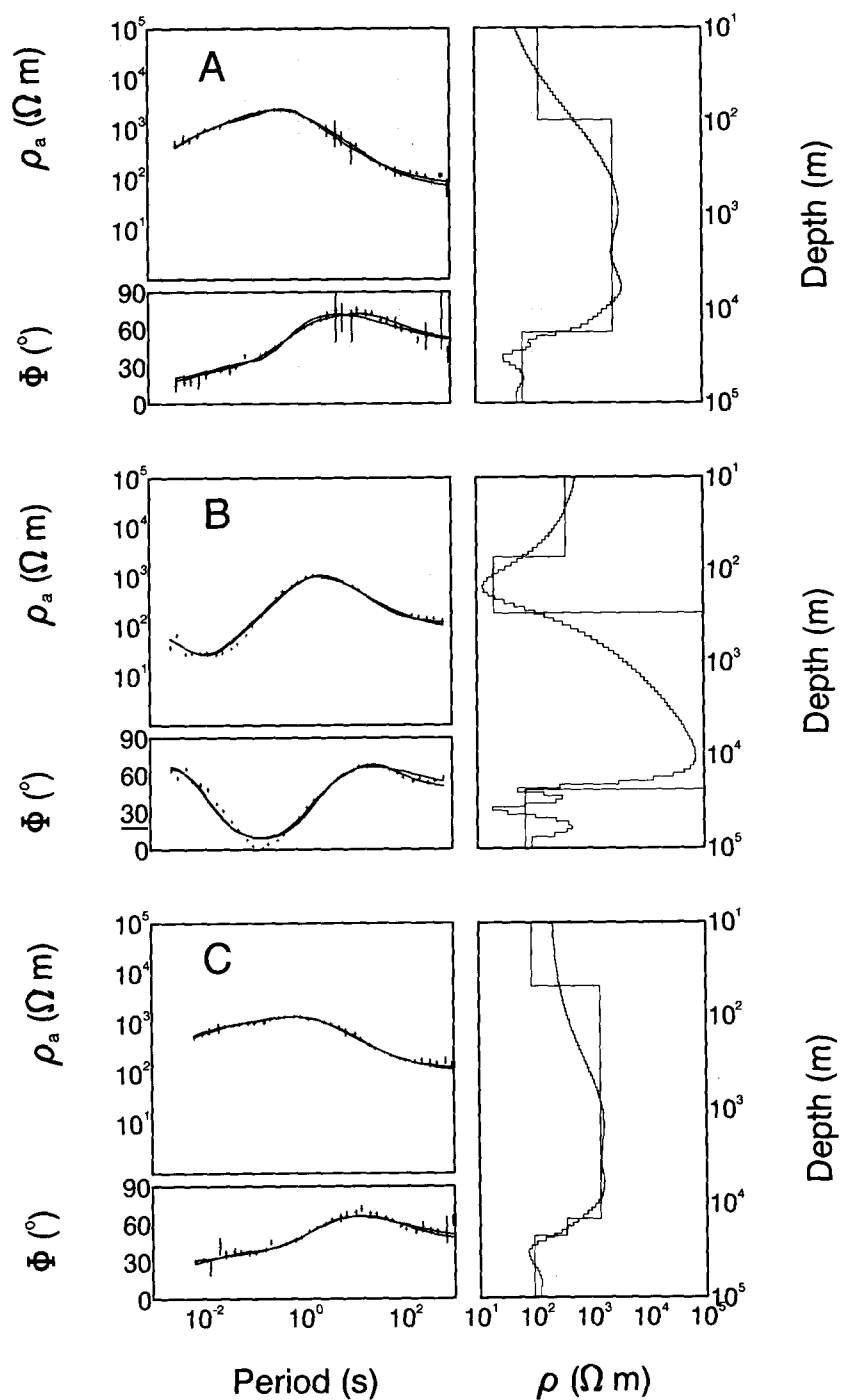


Fig. 14. 1D Occam inversions of the *E*-polarization data from a site on the flank of the belt (lit072, A), one on Mount Meager (mea004, B), and one on Mount Cayley (cay002, C).



Meager (mea004; Fig. 14(B)), and one on Mount Cayley (cay002; Fig. 14(C)). Also shown on the figures are layered-Earth inversions using the MINIM routine of Fischer and Le Quang (1981). Figure 15 shows the 1D Occam inversions, stitched together as a pseudo-2D model, from the Mount Meager sites with the six regional ones. Apparent in the inversions is the existence of a zone of enhanced electrical conductivity at depths of the order of 100 m beneath the Mount Meager and the eastern Mount Cayley sites, which is not apparent beneath either the regional sites or the western Mount Cayley ones.

Both the smooth and the layered-Earth inversions concur that there is a moderately resistive top layer, of some 80–100 m thick. Below this top layer sites on Mount Meager show the existence of a zone of enhanced conductivity, of some 20  $\Omega$  m, whereas this zone does not exist to the side of the mountain. For the regional sites, the upper crust is rather uniform with a resistivity of some 2500  $\Omega$  m, until depths of some 15–20 km at which there exists a layer of moderate resistivity (30–100  $\Omega$  m) underlying all sites.

The indication from the Meager sites is that the upper and middle crust beneath the conducting zone becomes extremely resistive, with values in excess of 50 000  $\Omega$  m. However, singular value decomposition analysis (e.g. Jones, 1982) of the

layered-Earth model shows that the resistivity of this resistive zone, sandwiched as it is between two conducting zones, is totally unresolved. Perhaps surprisingly, its thickness is the most well-resolved parameter, followed by the conductance (thickness times conductivity) of the shallow conducting zone.

From Fig. 15, we can already deduce that there exists a shallow conducting zone of limited lateral extent lying some 80–100 m beneath the surface of Mount Meager, and that it appears to be shallowest at its eastern end and dips to the west. Other features of the figure, such as lateral variation in the resistive upper-crustal zone and the basal conductive zone, require 2D modelling and inversion.

#### 4.2. 2D forward modelling

Having derived a pseudo-2D model from stitching together all the 1D responses, we used this as a starting model for trial-and-error 2D forward modelling of the data, concentrating on fitting preferentially the MT phase responses. There is high topographic variation in the region, especially around Mount Meager, which led Pham Van Ngoc (1980), and later Flores et al. (1985), to study theoretically the effect of topography with 2D models. These exercises showed that the in-

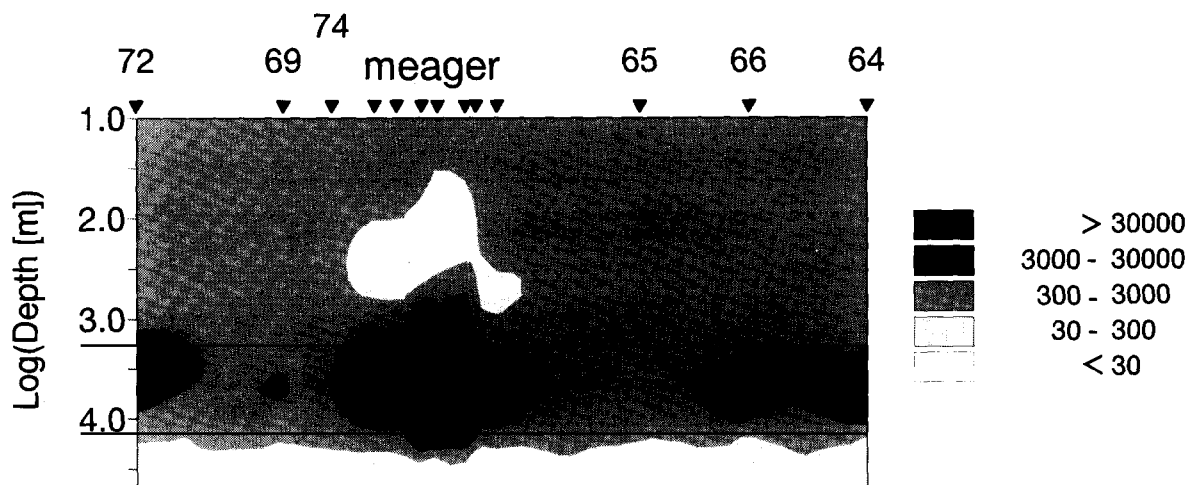


Fig. 15. Stitched 1D Occam inversions from the Mount Meager sites plus the six regional ones.

fluence of topography can be reasonably significant, especially for the *B*-polarization mode, with effects of up to 10% on  $\rho_a$  curves for a homogeneous earth. In our data, the influence on the MT results of conductivity structures dominates the responses, especially for the *E*-polarization data, and, accordingly, we neglected topography.

After many 2D models (over 100) were com-

puted and compared with the data responses, we consider the model shown in Fig. 16 to explain our observations best. The data and model  $\rho_a$  responses are compared in Fig. 17. The model shows essentially beneath the volcano a four-layer upper-crustal structure which is resistive–conductive–resistive–conductive from the surface. In contrast, off the volcano principally a two-layer

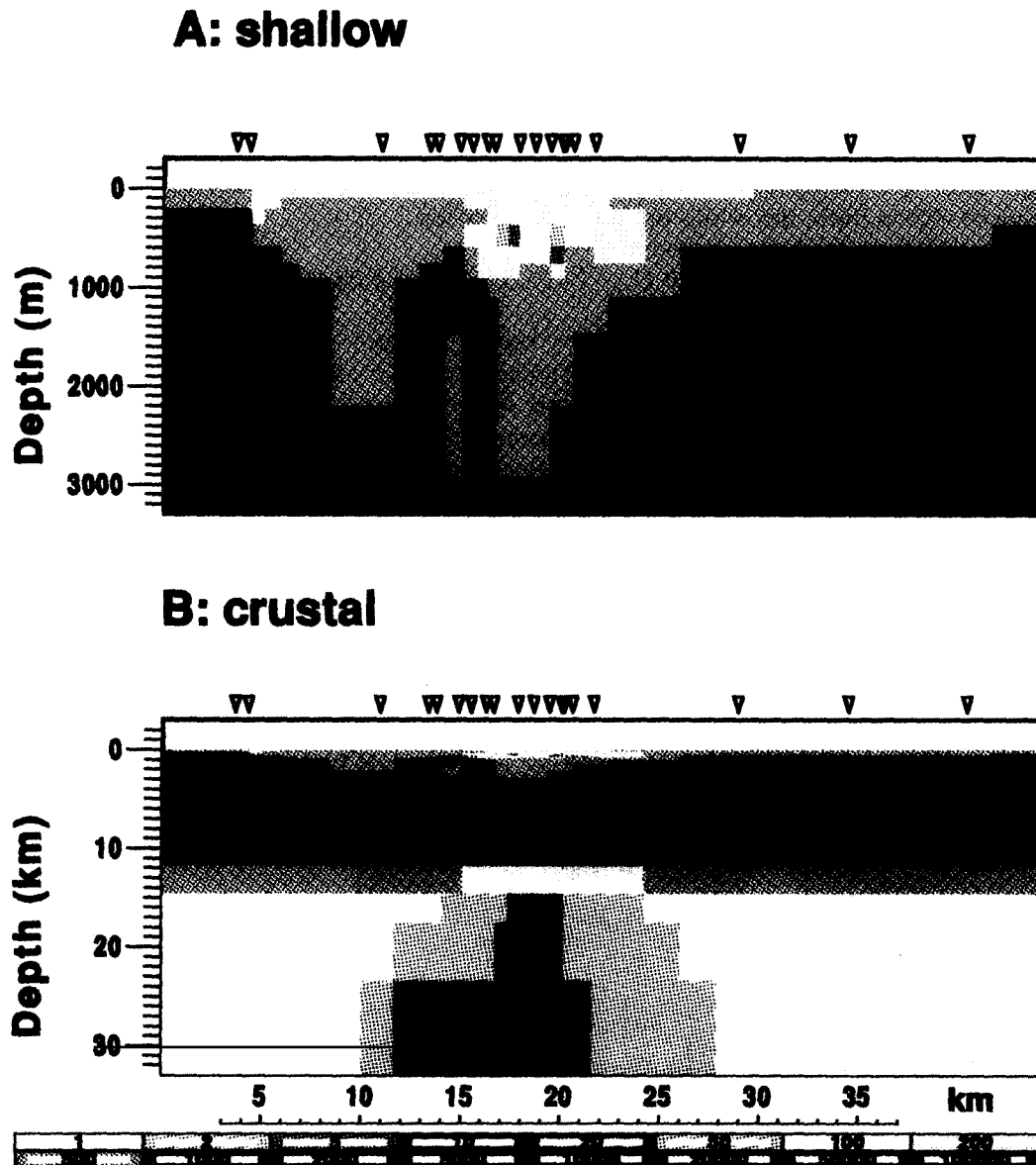


Fig. 16. Final 2D forward model obtained shown at two scales. (A) Uppermost 3000 m; (B) down to 30 km depth.

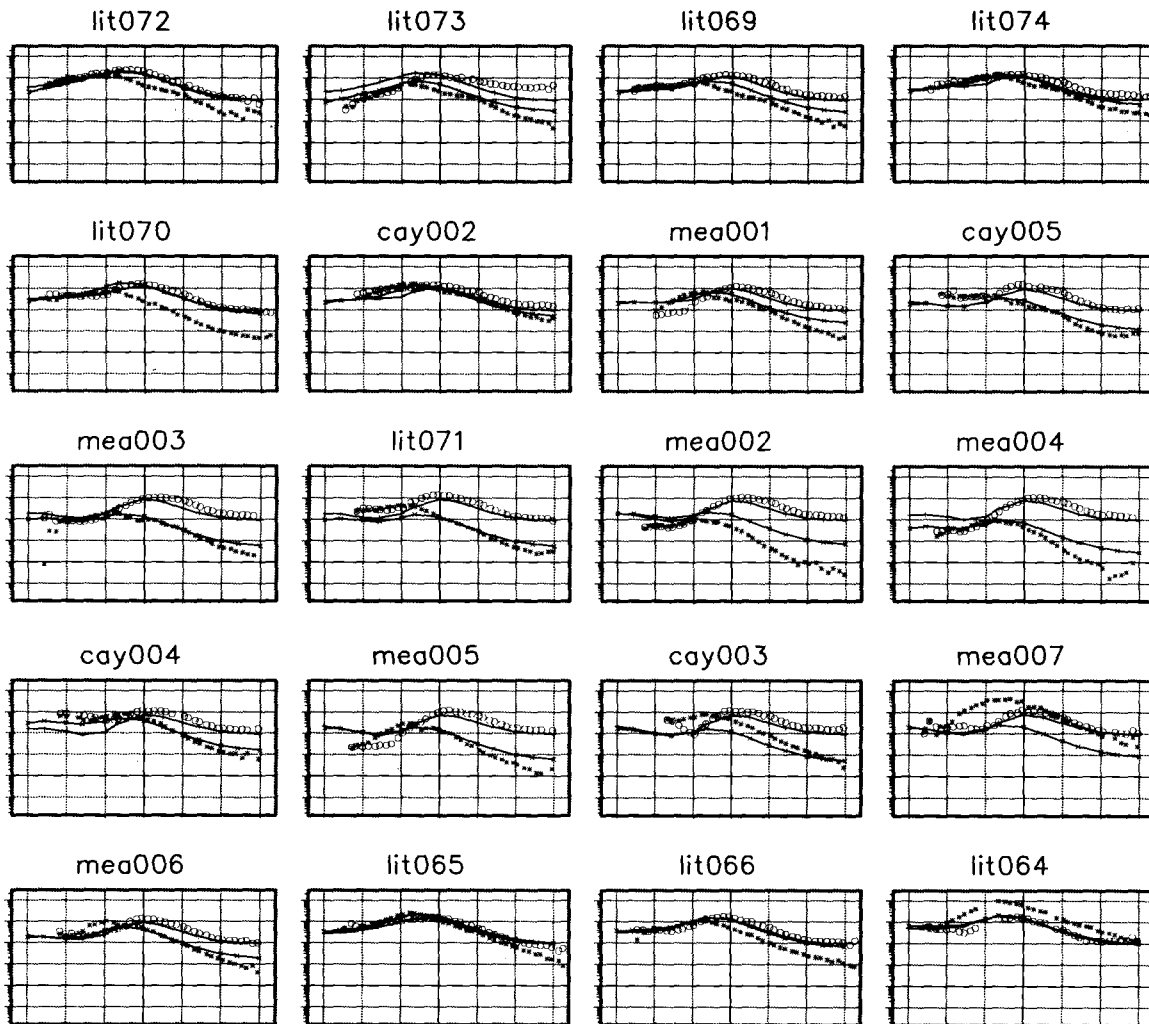


Fig. 17. MT  $\rho_a$  data and model responses from the model shown in Fig. 16.  $\circ$ ,  $E$ -polarization data;  $*$ ,  $B$ -polarization data. The solid lines are the model responses.

structure is found (resistive–conductive). We were not able to fit satisfactorily the very low, long-period,  $B$ -polarization resistivities, and their associated high phases, at Sites mea002 and mea004 without degrading the fit to the other data.

There is a zone of enhanced conductivity (20–80  $\Omega$  m) beneath the Mount Meager part of the Garibaldi volcanic belt. This zone has a width of 6 km and a depth extent of 500 m, and its top is at a depth of less than 200 m (Fig. 16, upper model). Between depths of 4–10 km, we have a uniformly highly resistive layer (from 4500 to more

than 30 000  $\Omega$  m) underlying the whole region. At depths in excess of 12 km, another conductive layer (100  $\Omega$  m) is modelled (Fig. 16, lower model). Within this layer there is a region of high conductivity (10  $\Omega$  m) directly beneath the volcanic belt. Sensitivity to this feature is principally in the  $B$ -polarization mode data; its exclusion degraded the fits at almost all sites.

A question which may be posed is whether our data require a connecting vertical ‘channel’ between the mid-crustal conductor and the geothermal zone to represent a magma conduit. Sensitiv-

ity to the existence of such a channel is in the period range of 0.1–1 s. The responses from many models with differing channel geometries and conductivities were computed, but the responses did not change significantly. Accordingly, we conclude that our data are insensitive to the presence of a moderately conducting thin vertical channel.

#### 4.3. 2D inversions

2D inversions of a reduced dataset were undertaken using the 2D Occam code of deGroot-

Hedlin and Constable (1990), with the addition of static shift determination by deGroot-Hedlin (1991). The dataset was reduced to all Mount Meager sites plus the regional LITHOPROBE sites because of the differences in internal conductivity structure between Mounts Cayley and Meager.

##### Shallow section

Figure 18 shows results from four Occam inversions for the shallow structure beneath Mount Meager (less than 1500 m depth) (note the vertical exaggeration of 7:1). Data at seven frequen-

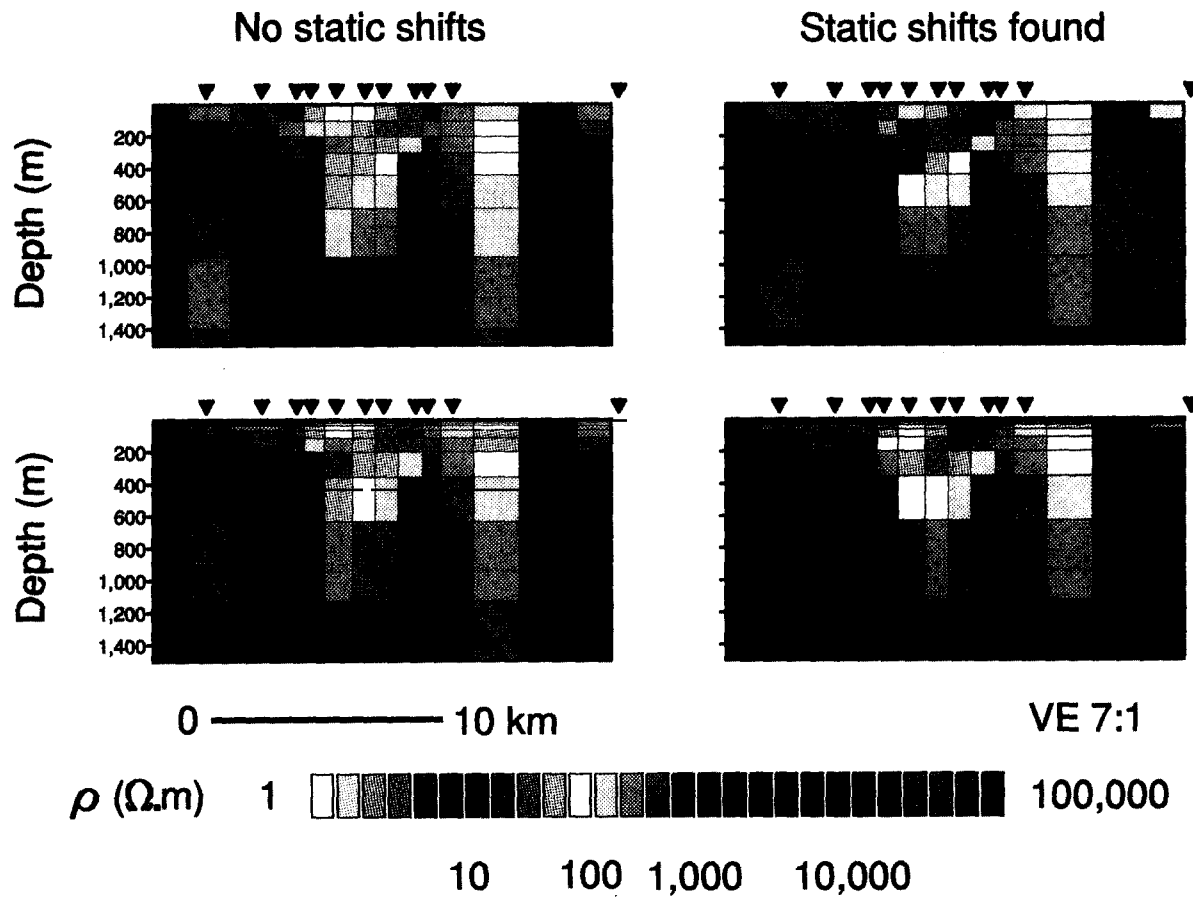


Fig. 18. Occam inversions for the shallow structure using both *E*-polarization and *B*-polarization resistivities and phases, as well as the transfer functions, from seven frequencies in the range 100 Hz–10 s from 14 sites (the seven Mount Meager sites plus cay002 and the six regional sites). (Only the central parts of the models are shown.) The two rows are for different regularization grids. The models in the left column are from inversions assuming that the static shifts had been corrected by requiring the long-period *E*-polarization  $\rho_a$  data to pass through 600  $\Omega$  m at 10 s. The models in the right column were obtained by allowing the Occam code to determine them.

cies were used, in the range 100 Hz–10 s, from both MT modes and including the vertical field transfer functions from 14 sites (a total of 588 data). These were all seven Meager sites, the six regional sites, and cay002. The two rows of models represent two different regularization grids, with the upper row starting at 100 m thickness and having six layers per decade in depth, and the lower row starting at 10 m and having four layers per decade, to test sensitivity to gridding. The two models on the left are obtained assuming that the static shifts have been correctly accounted for by shifting the MT  $\rho_a$  curves so that the  $E$ -polarization  $\rho_a$  data have the same long-period asymptote of 600  $\Omega$  m at 10 s. The two models on the right display inversions where the static shifts have been solved for as part of the inversion, using the algorithm of deGroot-Hedlin (1991). The  $\rho_a$  data for each site and for each mode are allowed to vary their levels (but obviously not their shapes), which leads to non-uniqueness unless some constraint is imposed. The physical constraint used by deGroot-Hedlin (1991) is that the static shifts derived for each mode must sum to zero, which is based on the asymptotic limit of a spatially sampled Earth overlaid by a random media thin sheet (see, e.g. Groom and Bailey, 1989b). Thus, the assumption is that for a sufficiently large number of MT sites the ensemble static shifts will appear as a zero-mean random perturbation. Where the number of sites is small, or where there may be a large inherent bias (e.g. sites on the Nelson batholith, Jones et al., 1992a), there may be a problem with this approach. Also, given that we do not measure point electric fields but measure potential differences between two points typically some 100 m apart, for the  $E$ -polarization mode the downward shift as a result of conductive inclusions is greater than the upward shift as a result of resistive ones, with the converse being true for the  $B$ -polarization mode (Jones, 1988), which may also lead to a bias.

The misfits of these four models are all around one; this result, given the error levels of the data, means that the models fit the data to within 2° in phase, 0.017 in  $\log(\rho_a)$ , and 0.05 in transfer function. All final models show the same geometry of

the conducting zone, with it being very close to the surface at its eastern edge then dipping to a depth of about 300 m. The zone has a resistivity minimum of around 10  $\Omega$  m.

#### *Regional structure*

The models of regional structure from Occam inversion of a reduced dataset of 10 sites (the regional and Meager sites excluding mea003 and mea004) have the same major features as the forward model illustrated in Fig. 16 (lower model). The Occam models did prefer to have the upper crust beneath the volcanic front less resistive, i.e. some thousands rather than some hundreds of thousands of ohm metres, than the model in Fig. 16. This may be an artefact of the Occam algorithm, or, more likely, it is a reflection of the inability of the data to resolve the resistivity of that region, save to state that it is resistive and to know its minimum resistivity.

### **5. Interpretation**

In 1977 four geothermal drill holes were completed in the Coast Mountains area, and all four holes indicated linear bottom hole temperature gradients approximately double the normal terrestrial geothermal gradient (Lewis, 1978). Follow-up shallow boreholes drilled in the early 1980s confirmed these findings (Bentkowski and Lewis, 1982). The existence of conductive zones at relatively shallow depth is in harmony with the high geothermal gradients found in these regions.

Beneath the South Thermal Reservoir of Mount Meager, and beneath the eastern side of Mount Cayley (Sites cay003 and cay004), are shallow (200 m) zones of enhanced electrical conductivity. The Mount Meager zone has been characterized and is closer to the surface on its eastern side than on its western side.

Many volcanoes in Japan have the same electrical features as Mount Meager, with the same resistivities and depths as our models. Deep drilling studies showed clay alteration minerals between 500 m and 2 km. The dominant clay alteration minerals are montmorillonite for the sealing cap rocks, and chlorite and sericite for the reservoir formation (Uchida, 1990).

We do not agree with others in interpreting these shallow conducting zones as due to magma chambers (Pham Van Ngoc, 1980), saline-fluid saturated granite (DeLaurier, 1986), or the hydrothermal zone itself (Flores-Luna, 1986). We conclude that our conductivity zones are also due to a clay layer with montmorillonite as the dominant clay alteration mineral. Montmorillonite is formed in a low-pressure and low-temperature environment (50–200°C) at borders of geothermal water circulation or by hydrolysis of volcanic ash, volcanic glass, and volcanic foam. It has very low resistivity (5–100  $\Omega$  m) and low permeability when it contains plenty of water, and forms an electrically conductive sealing cap rock.

A geothermal reservoir formation exists beneath this cap rock, with chlorite and sericite as the dominant clay alteration minerals. Chlorite and sericite are more resistive, which is consistent with our data (135–220  $\Omega$  m). However, high-temperature clay minerals such as chlorite and sericite seem not to decrease the resistivity of host rocks and or to seal fractures (Uchida, 1990).

The high values of resistivity (more than 10 000  $\Omega$  m) in the mid-layer (4–9 km) can be associated with the granitic and metamorphic Coast plutonic complex of granodiorite, diorite, quartz diorite, and other associated gneiss. Directly beneath the volcanic range there is the indication, from the 2D Occam inversions and from our 2D forward modelling exercise, that there may be a lowering of the resistivity to some thousands of ohm metres from tens of thousands of ohm metres. Within this there may exist a narrow vertical conduit for magma to flow from the source body to the surface. However, the resistivity in this channel cannot be lower than 1000  $\Omega$  m, or wider than a few kilometres, or we would be able to sense it. We note that Stanley et al. (1987) also did not detect a magma conduit beneath Mount St. Helens. In contrast, the model of Mozley et al. (1986) from data across Mount Hood, Oregon, includes a narrow (4 km wide), conducting (3  $\Omega$  m) channel electrically connecting a deep, highly conducting body to a surface conductor.

The enhanced electric conductivity at depths in excess of 12 km is probably related to the presence of free saline water which is derived

from waters driven off by metamorphic devolatilization of the downgoing Juan de Fuca plate to the west. Caner (1971) concluded that the enhanced conductivity of the lower crust is due to hydration or partial melting and is a characteristic feature of the entire western Cordillera. Large amount of free water are generated by dehydration reactions in the downgoing oceanic crust, and progressive dehydration will occur, particularly at temperatures above about 300–400°C (e.g. Fyfe et al., 1978). The water migrates upward until reduced temperature results in hydration reactions and mineral precipitation, forming an impermeable layer that traps the fluid horizon below (Etheridge et al., 1983; Jones, 1987). Lewis et al. (1988) estimated that crustal dehydration will produce water between depths of 18–60 km above the downgoing slab, and that the hydration boundary, mapped at depths of 25–35 km beneath Vancouver Island by Kurtz et al. (1986, 1990), will rise abruptly to some 20 km beneath the Garibaldi volcanic belt, which agrees well with our own interpretation. Also, regional interpretation of MT data in the Coast belt suggested a resistivity of 150  $\Omega$  m below 14 km (Jones et al., 1992a), and modelling of data from 80–100 km further east across the Fraser River fault gave a lower crust with a resistivity of 100  $\Omega$  m below 20–23 km beneath the Coast belt side of the fault (Jones et al., 1992b). Using a value of 50  $S\ m^{-1}$  for the saline fluid, and assuming that the host rock is of sufficiently high relative resistivity that it can be ignored, leads to porosities of 1.4% using Archie's Law with an exponent of two (see, e.g. Jones, 1992).

Within this conducting layer is a region of high conductivity modelled with a resistivity of 10  $\Omega$  m beginning at a depth of some 14 km (Fig. 16; lower model). Under most of the Cascade Range, where volcanism has occurred over the last 2–5 m.y., a zone of magma interception, storage, and crystallization is thought to exist in the depth range of 8–15 km (Blackwell et al., 1990), which is in agreement with our own depth estimate for the highly conductive region. Accordingly, we interpret this zone as the source magma body beneath the Garibaldi volcanic belt, which is at

variance with the conclusion in a recent review of EM studies in geothermal fields by Martinez-Garcia (1992) that magma chambers are not being detected by EM methods.

Jiracek et al. (1983) suggested that some magma chambers might not be conductive features, contrary to what one would expect from laboratory studies of melting (Tyburczy and Waff, 1983), as their interpretations led them to propose that the Socorro magma body in the Rio Grande rift is not conductive. Hermance and Neumann (1991) recently challenged the interpretation of Jiracek et al. (1983) showing that their own data require a well-resolved conducting body of some  $6 \Omega \text{ m}$  ( $2\text{--}16 \Omega \text{ m}$ ) at a depth of 20 km with a width of 25 km and a thickness extent of 10 km. We note that our body has a resistivity of  $10 \Omega \text{ m}$ , which is close to that of the Socorro body of  $6 \Omega \text{ m}$  modelled by Hermance and Neumann (1991).

A LITHOPROBE seismic reflection profile close to Mount Cayley found a seismic 'bright spot'—band of high-amplitude reflectors of 10 km width and 0.3 s thickness—at 4.5 s two-way time. R.M. Clowes (personal communication (1991) reported by Lewis et al. (1992)) suggested that the reflection source lies off-line. If the source lies below Mount Cayley, it would be at a depth of 11 km, which is the interpreted top of the fluid-saturated region (Fig. 16). Alternatively, our modelled depth to the top of the magma chamber (14.5 km; Fig. 16) may be in error by 25% and the bright spot may be the top of the magma chamber. For this to be the case, however, our static shifts would have to be in error by almost a factor of two, which is possible but not likely.

## 6. Conclusions

Modelling and inversion of high-quality MT data collected across two volcanic mounts, combined with data from regional sites, has permitted us to characterize the electrical structure of the Garibaldi volcanic front. The features of our model (Fig. 16), and our interpretation of these features, are as follows:

(1) there is a near-surface conductive region beneath all of Mount Meager and the eastern part of Mount Cayley at a depth of some 100–500 m. The conductor dips to the west beneath Mount Meager. We interpret this conductor as being due to montmorillonite-dominated clay alteration minerals which form the cap rock to the geothermal reservoir.

(2) Beneath this conductor is a relatively resistive region, which is the geothermal reservoir formation itself.

(3) The upper crust is very resistive (more than  $1000 \Omega \text{ m}$ ) beneath the whole of the belt. However, we cannot preclude the existence of a narrow (less than 3 km width), relatively conductive (some hundreds of ohm metres) vertical channel directly beneath the front.

(4) At depths of 12 km the resistivity decreases to a value of some  $100 \Omega \text{ m}$ . We interpret this layer as the result of conduction in saline fluids, in a matrix of 1–2% porosity, expelled by the downgoing Juan de Fuca plate to the west.

(5) Beneath the Garibaldi volcanic belt is a region of enhanced conductivity ( $10 \Omega \text{ m}$ ) in the middle and lower crust starting at 14.5 km. We interpret this as the magma source body for the belt.

## Acknowledgements

Discussions with Toshi Uchida and constructive reviews by Jim Craven and Gary McNeice are gratefully acknowledged. Gaston Fischer and Steve Constable provided the 1D inverse codes, and Steve Constable and Catherine deGroot-Hedlin the 2D inverse code. The 2D forward modelling was undertaken using Phil Wannamaker's code as implemented as part of the Geotools Plus package of WSE Associates. The Mount Meager data were collected by Ron Kurtz and Jon DeLaurier, whereas the Mount Cayley data were acquired by Phoenix Geophysics (Toronto) Ltd. under the auspices of the Federal Geothermal Energy Program. The LITHOPROBE data were also acquired by Phoenix, who are thanked for their attention to detail which resulted in high-quality MT responses. Catherine

Hickson is thanked for providing a digital graphics file from which Figs. 1 and 2 were constructed. This paper is Geological Survey of Canada Contribution 46792 and LITHOPROBE Publication 428.

### Note added in proof

It has been brought to our attention during the proof-reading stage that the vertical field magnetometer at Site mea003 was lying horizontally during data acquisition (R.D. Kurtz, personal communication, 1993). Accordingly, the anomalously large induction vector for this site on Fig. 4 should be ignored. Removing the transfer function data from this site was found to have little influence on the models shown in Fig. 18.

### References

- Bahr, K., 1988. Interpretation of the magnetotelluric impedance tensor: regional induction and local telluric distortion. *J. Geophys.*, 62: 119–127.
- Bahr, K., 1991. Geological noise in magnetotelluric data: a classification of distortion types. *Phys. Earth Planet. Inter.*, 66: 24–38.
- Bentkowski, W.H. and Lewis, T.J., 1982. Preliminary results of shallow drilling in the Garibaldi volcanic belt, British Columbia. Earth Physics Branch Open File 83–23, Earth Physics Branch, Dept. EMR, Ottawa, 57 pp.
- Berdichevsky, M.N., Vanyan, L.L. and Dmitriev, V.I., 1989. Methods used in the U.S.S.R. to reduce near-surface inhomogeneity effects on deep magnetotelluric sounding. *Phys. Earth Planet. Inter.*, 53: 194–206.
- Blackwell, D.D., Steele, J.L., Kelley, S. and Korosec, M.A., 1990. Heat flow in the state of Washington and thermal conditions in the Cascade Range. *J. Geophys. Res.*, 95: 19495–19516.
- Caner, B., 1971. Quantitative interpretation of geomagnetic depth sounding data in western Canada. *J. Geophys. Res.*, 76: 7202–7216.
- Cassidy, J.F. and Ellis, R.M., 1991. Shear wave constraints on a deep crustal reflective zone beneath Vancouver Island. *J. Geophys. Res.*, 96: 19843–19851.
- Cassidy, J.F. and Ellis, R.M., 1993. *S*-velocity structure of the northern Cascadia subduction zone. *J. Geophys. Res.*, 98: 4407–4421.
- Chakraborty, R., Chouteau, M. and Mareschal, M., 1992. A simple technique for analysing and partly removing galvanic distortion from the magnetotelluric impedance tensor: application to Abitibi and Kapuskasing data (Canada). *Geophys. J. Int.*, 108: 917–929.
- Clague, J.J., 1989. Quaternary geology of the Canadian Cordillera. In: R.J. Fulton (Editor), *Quaternary Geology of Canada and Greenland. Geology on Canada*, No. 1. Geol. Surv. Can., pp. 15–96.
- Clowes, R.M., Yorath, C.J. and Hyndman, R.D., 1987. Reflection mapping across the convergent margin of western Canada. *Geophys. J.R. Astron. Soc.*, 89: 79–84.
- Constable, S.C., Parker, R.L. and Constable, C.G., 1987. Occam's inversion: a practical algorithm for generating smooth models from electromagnetic sounding data. *Geophysics*, 52: 289–300.
- deGroot-Hedlin, C., 1991. Removal of static shift in two dimensions by regularized inversion. *Geophysics*, 56: 2102–2106.
- deGroot-Hedlin, C. and Constable, S., 1990. Occam's inversion to generate smooth two-dimensional models from magnetotelluric data. *Geophysics*, 55: 1613–1624.
- DeLaurier, J.M., 1986. Magnetotelluric sounding near Cayley mountain. Pacific Geoscience Centre Internal Report, Geol. Surv. Canada, Dept. EMR, Sydney, 11 pp.
- Dragert, H., Law, L.K. and Sule, P.O., 1980. Magnetotelluric soundings across the Pemberton Volcanic Belt, British Columbia. *Can. J. Earth Sci.*, 17: 161–167.
- Eggers, D.E., 1982. An eigenstate formulation of the magnetotelluric impedance tensor. *Geophysics*, 47: 1204–1214.
- Etheridge, M.A., Wall, V.J. and Vernon, R.H., 1983. The role of the fluid phase during regional metamorphism and deformation. *J. Metamorphic Geol.*, 1: 205–226.
- Fischer, G. and Le Quang, B.V., 1981. Topography and minimization of the standard deviation in one-dimensional magnetotelluric modelling. *Geophys. J.R. Astron. Soc.*, 67: 279–292.
- Flores, C., Kurtz, R.D. and DeLaurier, J., 1985. Magnetotelluric exploration in the Meager Mountain Geothermal Area, Canada. *Acta Geodaet., Geophys. Mont. Acad. Sci. Hung.*, 20: 165–171.
- Flores-Luna, C., 1986. Electromagnetic induction studies over the Meager Creek geothermal area, British Columbia. Ph.D. Thesis, Department of Physics, University of Toronto.
- Fyfe, W.S., Price, N.J. and Thompson, A.B., 1978. *Fluids in the Earth's Crust*. Elsevier, Amsterdam, 383 pp.
- Gabriele, H. and Yorath, C.J., 1989. The Cordilleran orogen in Canada. *Geosci. Can.*, 16: 62–83.
- Gordienko, V.V., Kulik, S.N. and Logvinov, I.M., 1981. Asthenosphere of Epi-Hercynian platforms. *Geophys. J.*, 3: 202–216.
- Green, N.L., Armstrong, R.L., Harakal, J.E., Souther, J.G. and Read, P.B., 1988. Eruptive history and K–Ar geochronology of the Garibaldi volcanic belt, southwestern British Columbia. *Geol. Soc. Am. Bull.*, 100: 563–579.
- Groom, R.W. and Bahr, K., 1992. Corrections for near surface effects: decomposition of the magnetotelluric impedance tensor and scaling corrections for regional resistivities: a tutorial. *Geophys. Surv.*, 13: 341–380.
- Groom, R.W. and Bailey, R.C., 1989a. Decomposition of magnetotelluric impedance tensor in the presence of local



- three-dimensional galvanic distortion. *J. Geophys. Res.*, 94: 1913–1925.
- Groom, R.W. and Bailey, R.C., 1989b. Some effects of multiple lateral inhomogeneities in magnetotellurics. *Geophys. Prospect.*, 37: 697–712.
- Groom, R.W. and Bailey, R.C., 1991. Analytical investigations of the effects of near-surface three-dimensional galvanic scatterers on MT tensor decomposition. *Geophysics*, 56: 496–518.
- Groom, R.W., Kurtz, R.D., Jones, A.G. and Boerner, D.E., 1993. A quantitative methodology for determining the dimensionality of conductive structure from magnetotelluric data. *Geophys. J. Int.*, in press.
- Hermance, J.F. and Neumann, G.A., 1991. The Rio Grande rift: electromagnetic constraints on the Socorro magma body. *Phys. Earth Planet. Inter.*, 66: 101–117.
- Hickson, C.J., 1993. Volcanism in the Canadian cordillera. *Proc. 1st Int. Symp. on Volcanic Ash and Aviation Safety*, in press.
- Hyndman, R.D., 1988. Dipping seismic reflectors, electrically conductive zones, and trapped water in the crust over a subducting plate. *J. Geophys. Res.*, 93: 13391–13405.
- Hyndman, R.D., Yorath, C.J., Davis, E.E. and Clowes, R.M., 1990. The northern Cascadia subduction zone at Vancouver Island: the structure and tectonic history. *Can. J. Earth Sci.*, 27: 313–329.
- Jiracek, G.R., Gustafson, E.P. and Mitchell, P.S., 1983. Magnetotelluric results opposing magma origin of crustal conductors in the Rio Grande Rift. *Tectonophysics*, 94: 299–326.
- Jones, A.G., 1982. On the electrical crust–mantle structure in Fennoscandia: no Moho and the asthenosphere revealed? *Geophys. J.R. Astron. Soc.*, 68: 371–388.
- Jones, A.G., 1986. Parkinson's pointers' potential perfidy! *Geophys. J.R. Astron. Soc.*, 87: 1215–1224.
- Jones, A.G., 1987. MT and reflection: an essential combination. *Geophys. J.R. Astron. Soc.*, 89: 7–18.
- Jones, A.G., 1988. Static shift of magnetotelluric data and its removal in a sedimentary basin environment. *Geophysics*, 53: 967–978.
- Jones, A.G., 1992. Electrical conductivity of the continental lower crust. In: D.M. Fountain, R.J. Arculus and R.W. Kay (Editors), *Continental Lower Crust*. Elsevier, Amsterdam, pp. 81–143.
- Jones, A.G. and Groom, R.W., 1993. Strike angle determination from the magnetotelluric tensor in the presence of noise and local distortion: rotate at your peril! *Geophys. J. Int.*, 113: 524–534.
- Jones, A.G., Gough, D.I., Kurtz, R.D., DeLaurier, J.M., Boerner, D.E., Craven, J.A., Ellis, R.G. and McNeice, G.W., 1992a. Electromagnetic images of regional structure in the southern Canadian cordillera. *Geophys. Res. Lett.*, 12: 2373–2376.
- Jones, A.G., Kurtz, R.D., Boerner, D.E., Craven, J.A., McNeice, G., Gough, D.I., DeLaurier, J.M. and Ellis, R.G., 1992b. Electromagnetic constraints on strike-slip fault geometry—the Fraser River fault system. *Geology*, 20: 561–564.
- Krasnobayeva, A.G., D'Yakonov, B.P., Astaf'yev, P.F., Batalova, O.V., Vishnev, V.S., Gavrilova, I.E., Zhuravleva, P.B. and Kirillov, S.K., 1981. Electromagnetic experiments on the Baltic Shield. *Izv. Earth Phys.*, 17: 439–444.
- Kurtz, R.D., DeLaurier, J.M. and Gupta, J.C., 1986. A magnetotelluric sounding across Vancouver Island sees the subducting Juan de Fuca plate. *Nature*, 321: 596–599.
- Kurtz, R.D., DeLaurier, J.M. and Gupta, J.C., 1990. The electrical conductivity distribution beneath Vancouver Island: a region of active plate subduction. *J. Geophys. Res.*, 95: 10929–10946.
- LaTorraca, G.A., Madden, T.R. and Korrington, J., 1986. An analysis of the magnetotelluric impedance for three-dimensional conductivity structures. *Geophysics*, 51: 1819–1829.
- Lewis, J.F., 1978. Preliminary field report of drilling near Mount Meager and Mount Cayley volcanic centres. *Earth Physics Branch Open File 78–2*, Earth Physics Branch, Dept. EMR, Ottawa, 25 pp.
- Lewis, T.J. and Souther, J.G., 1978. Meager Mountain, B.C. A possible geothermal energy resource. *Earth Physics Branch, Dept. EMR, Ottawa, Geothermal Ser.*, 9, 17 pp.
- Lewis, T.J., Bentkowski, W.H., Hyndman, R.D., Souther, J.G. and Wright, J.A., 1988. Subduction of the Juan de Fuca plate: thermal consequences. *J. Geophys. Res.*, 93: 15207–15225.
- Lewis, T.J., Bentkowski, W.H. and Hyndman, R.D., 1992. Crustal temperatures near the LITHOPROBE Southern Cordilleran Transect. *Can. J. Earth Sci.*, 29: 1197–1214.
- Martinez-Garcia, M., 1992. Electromagnetic induction in geothermal fields and volcanic belts. *Surv. Geophys.*, 13: 409–434.
- Monger, J.W.H., 1989. Overview of Cordilleran geology. In: B.D. Ricketts (Editor), *Western Canada Sedimentary Basin*. Can. Soc. Petrol. Geol., Calgary, pp. 9–32.
- Mozley, E.C., Goldstein, N.E. and Morrison, H.F., 1986. Magnetotelluric investigations at Mount Hood, Oregon. *J. Geophys. Res.*, 91: 11596–11610.
- Parkinson, W.D., 1962. The influence of continents and oceans on geomagnetic variations. *Geophys. J.R. Astron. Soc.*, 6: 441–449.
- Pham Van Ngoc, 1977. Magnetotelluric reconnaissance survey in the Lillooet Valley, B.C. *Earth Physics Branch Open File 77–20*, Earth Physics Branch, Dept. EMR, Ottawa, 40 pp.
- Pham Van Ngoc, 1978. Magnetotelluric prospecting in the Mount Meager Geothermal Region. *Earth Physics Branch Open File 78–6E*, Earth Physics Branch, Dept. EMR, Ottawa, 31 pp.
- Pham Van Ngoc, 1980. Magnetotelluric survey of the Mount Meager and the region of the Squamish valley. *Earth Physics Branch Open File 80–8E*, Earth Physics Branch, Dept. EMR, Ottawa, 77 pp.
- Read, P.B., 1977. Meager Creek volcanic complex, southwest-

- ern British Columbia. *Curr. Res. Geol. Sur. Can. Pap.*, 77-1A: 277–281.
- Read, P.B., 1978. Geology, Meager Creek geothermal area, British Columbia. *Geol. Surv. Can. Open File* 603, Geol. Survey Canada, Dept. EMR, Ottawa.
- Read, P.B., 1990. Mount Meager complex, Garibaldi belt, southwestern British Columbia. *Geosci. Can.*, 17: 179–187.
- Richter, D.H., Smith, J.G., Lanphere, M.A., Dalrymple, G.B., Reed, B.L. and Shew, N., 1990. Age and progression of volcanism, Wrangell volcanic field, Alaska. *Bull. Volcanol.*, 53: 29–44.
- Riddihough, R.P., 1978. The Juan de Fuca Plate. *Eos*, 59: 836–842.
- Roddick, J.A., 1983. Geophysical review and composition of the Coast Plutonic Complex, south of latitude 55°N. *Geol. Soc. Am. Mem.*, 159: 195–212.
- Souther, J.G., 1986. The western Anahim Belt: root of a peralkaline magma system. *Can. J. Earth Sci.*, 23: 895–908.
- Souther, J.G., 1992. The Late Cenozoic Mount Edziza Volcanic Complex, British Columbia. *Geol. Surv. Can. Mem.* 420, Geol. Survey Canada, Dept. EMR, Ottawa, 320 pp.
- Spence, G.D., Clowes, R.M. and Ellis, R.M., 1985. Seismic structure across the subduction zone of western Canada. *J. Geophys. Res.*, 90: 6754–6772.
- Stanley, W.D., Finn, C. and Plesha, J.L., 1987. Tectonics and conductivity structures in the southern Washington Cascades. *J. Geophys. Res.*, 92: 10179–10193.
- Sternberg, B.K., Washburne, J.C. and Pellerin, L., 1988. Correction for the static shift in magnetotellurics using transient electromagnetic soundings. *Geophysics*, 53: 1459–1468.
- Swift, G.M., 1967. A magnetotelluric investigation of an electrical conductivity anomaly in the south-western United States. Ph.D. Thesis, Department of Geology and Geophysics, Massachusetts Institute of Technology, Cambridge, MA.
- Tyburczy, J.A. and Waff, H.S., 1983. Electrical conductivity of molten basalt and andesite to 25 kilobars pressure: geophysical significance and implications for charge transport and melt structure. *J. Geophys. Res.*, 88: 2413–2430.
- Uchida, T., 1990. Reservoir structure of the Sengan Geothermal Field interpreted from the resistivity data. *J. Geotherm. Res. Soc. Jpn.*, 12: 1–21.
- Vanyan, L.L., Yegorov, I.V., Shilovsky, P.P., Al'perovich, I.M., K'nikiforov, V.M. and Volkova, O.V., 1983. Characteristics of deep electrical conductivity of Northern Sakhalin. *Izv. Earth Phys.*, 19: 208–214.
- Vanyan, L.L., Shilovsky, A.P., Okulesky, B.A., Semenov, V.Y. and Sidelnikova, T.A., 1989. Electrical conductivity of the crust of the Siberian platform. *Phys. Earth Planet. Inter.*, 54: 163–166.
- Warner, B.N., Bloomquist, M.G. and Griffith, P.G., 1983. Magnetotelluric interpretations based upon new processing and display techniques: Contributed paper at the 53rd Ann. Int. Mtg., Soc. Explor. Geophys., Las Vegas, 11–15 September, Expanded Abstracts, pp. 151–154.
- Yee, E. and Paulson, K.V., 1987. The canonical decomposition and its relationship to other forms of magnetotelluric impedance tensor analysis. *J. Geophys.*, 61: 173–189.
- Zhang, P., Roberts, R.G. and Pedersen, L.B., 1986. Magnetotelluric strike rules. *Geophysics*, 52: 267–278.